Clays and Clay Minerals, Vol. 64, No. 5, 608–627, 2016.

ILLITE-SMECTITE-RICH CLAY PARAGENESES FROM QUATERNARY TUNNEL VALLEY SEDIMENTS OF THE DUTCH SOUTHERN NORTH SEA – MINERAL ORIGIN AND PALEOENVIRONMENT IMPLICATIONS

Branimir Šegvić*, Antonio Benvenuti, and Andrea Moscariello

Department of Earth Sciences, University of Geneva, 13 Rue des Maraîchers, 1205 Geneva, Switzerland

Abstract—The Pleistocene sediment infill of elongated glacial incisions of the southern North Sea (SNS) is often referred to as tunnel valleys (TVs). The depositional environment is not yet fully understood and the present study addresses this challenge from the perspective of clay-mineral transformation (illite to illite-smectite) reported from the largest Elsterian TV of the SNS. Material acquired from the K14-12 borehole in the Dutch offshore was analyzed by X-ray diffraction (XRD), electron microscopy, electron microprobe, and laser particle-size analysis. Illite and illite-smectite (I-S) appeared as dominant clays along with minor amounts of kaolinite, kaolinite-smectite, and chlorite. The largest amount of I-S is recognized in the main TV portion, while in pre-glacial and uppermost deposits, I-S is less abundant. The XRD peak fitting and deconvolution suggest that I-S consists of several intermediates – ordered (well crystallized illite + R3 I-S) and disordered (R0 I-S + R0 I-SS). Given the average particle sizes (>2 μm) and Kübler index values (0.415−0.341°Δ2θ), illite as well as chlorite and kaolinite were interpreted as detrital. On the basis of the distinctive distribution, grain sizes, and compositional variations of I-S, formation by means of early diagenetic *in situ* smectitization of illite under a cold climate is proposed. The process operated *via* a series of mixed-layer intermediates derived from an illite component being converted progressively to low-charged smectite. The reaction is marked by a significant net loss of K and Al with replacement by Si in a tetrahedral coordination. Layer-charge imbalance is accommodated by Fe(III) and Mg entering an octahedral sheet, whereas Ca partly fills the interlayer sites. Smectitization rates were controlled by illite grain sizes. The results of the present study support strongly the existence of an ice-marginal freshwater depositional environment at the glacial maximum in the SNS in which early diagenesis at low temperatures resulted in incomplete conversion of illite to smectite.

Key Words—Diagenesis, Illite-smectite, Middle Pleistocene, Proglacial Lake, Tunnel Valley, Smectitization, Southern North Sea.

INTRODUCTION AND GEOLOGICAL SETTING

A large number of elongated glacial incisions known as 'tunnel valleys' formed under subglacial conditions at former ice-margins of the Quaternary ice-sheets (Figure 1; Laban, 1995; Praeg, 1996; Huuse and Lykke-Andersen, 2000; Kehew *et al.*, 2012; Moreau *et al.*, 2012; van der Vegt *et al.*, 2012), which repeatedly occupied the North Sea over the last 1 million years (Huuse and Lykke-Andersen, 2000; Ehlers and Gibbard, 2004). The largest and deepest TVs in the southern North Sea (SNS, Figure 2a) are generally referred to as the Elsterian glaciation (dated at marine isotope stage (MIS) 12: 480−420 ka according to Cohen and Gibbard (2010); MIS 10: 390−340 ka according to Lee *et al.* (2012)), when British and Scandinavian ice-sheets covered the majority of the SNS (*e.g.* Mangerud and Jansen, 1996). Most of the SNS TVs share common clinoform sandy-silty-clayey infill (Figure 2b) thought to represent either reworked preglacial or new Quaternary sediments (Praeg, 1996; Moreau and Huuse, 2014; Benvenuti and Moscariello, 2016). The focus of this study is the sediments of the largest Elsterian TV of the SNS (Figure 2), in particular the mineralogy and geochemistry of the clay-mineral content, crucial for a better understanding of depositional paleoenvironments and early diagenetic processes involved in the clay-mineral formation.

During the majority of the Tertiary and Quaternary, the area of the SNS was exposed to the shallow marine sedimentation in which fine- to medium-grained sands prevailed (de Gans, 2007; de Lugt, 2007). The diversity of clay-mineral assemblages found in those sands reflected dominant fluvial systems that at the same time brought large amounts of sediments mainly from the East (Baltic, Scandinavia, Eastern Germany) and South (Central Europe) (Zagwijn, 1989; de Gans, 2007; Westerhoff, 2009). The material sourced from the East was transported by the Baltic River System (BRS, Figure

* E-mail address of corresponding author:
bsegvic@gmail.com
Current address: Department of Geosciences, Texas Tech University, Lubbock, TX 79409, USA

This paper is published as part of a special section on the subject of 'Clays in the Critical Zone,' arising out of presentations made during the 2015 Clay Minerals Society-Euroclay Conference held in Edinburgh, UK.

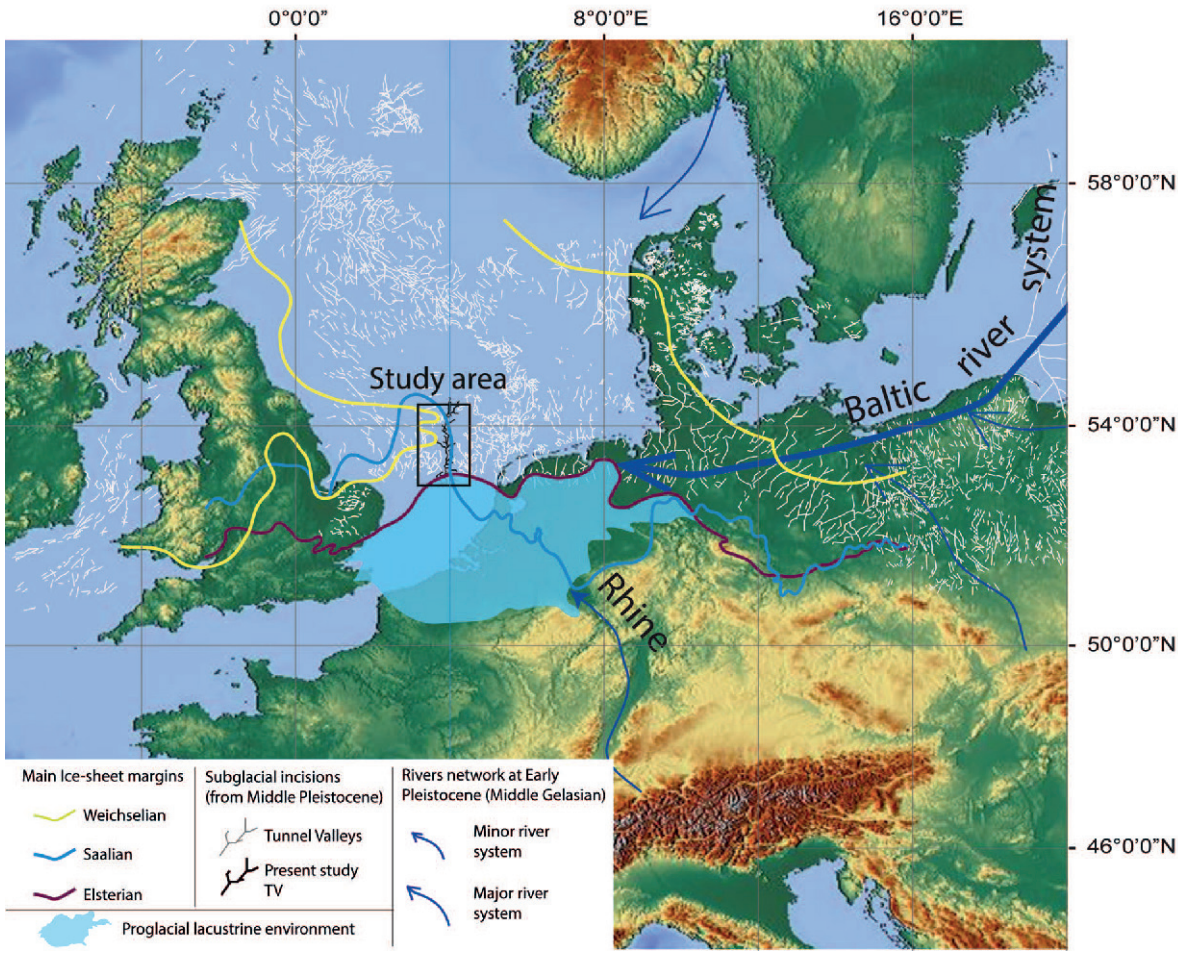

Figure 1. Schematic representation of the drainage system of the southern North Sea during the Early Pleistocene and the most significant features in terms of the successive glaciations (*i.e.* ice-sheet margins and TVs). The location of the study area is outlined in black. The main river systems are after de Gans (2007) and Westerhoff (2009) indicating the source areas of detrital material. Continuous lines in yellow, blue, and red indicate the positions of ice-margins at glacial maxima and are reproduced with the permission of the author, Philip Gibbard, from *www.qpg.geog.cam.ac.uk/research/projects/nweurorivers/*. The numerous tiny black lines and the red line in the study area indicate the large number of glacial incisions created during repeated glaciations in NW Europe and are redrawn after van der Vegt *et al.* (2012). The proglacial lacustrine environment created at the Elsterian glacial maximum is modified after Murton and Murton (2012).

1; Bijlsma, 1981; de Gans, 2007), which gave rise to the progressive filling of the whole SNS basin with sediments enriched in illite and kaolinite, and depleted in smectite during the Late Pliocene and the Early Pleistocene (Leipe and Sea, 2003; Kuhlmann *et al.*, 2004; Nielsen *et al.*, 2015). In contrast, the fine-grained sediment enriched in smectite was supplied largely by European rivers (Kuhlmann *et al.*, 2004; Adriaens, 2015; Griffioen *et al.*, 2016). Those became important in the Dutch SNS only by the upper Early Pleistocene when the BRS slowly ceased its activity (Zagwijn, 1989; de Gans, 2007; Westerhoff, 2009). Generally speaking, the Quaternary deposits of the SNS represent a mixture of many different sources and are dominated by illite and smectite along with their mixed-layer phases while kaolinite and chlorite are less abundant (Griffioen *et al.*, 2016 and references therein). In the fine fraction of the TV sediments analyzed, however, illite and illite-rich I-S (smectite content $\leqslant$31%) have been reported as the most common phases. Such a finding corresponds only partly to the existing literature data due to complete lack of discrete smectite and scarcity of smectite-rich mixed-layer clays (smectite content >50%; Irion and Zöllmer, 1999; Zuther *et al.*, 2000; Huggett and Knox, 2006; Adriaens, 2015; Griffioen *et al.*, 2016). Hence, the clays of the Elsterian TV investigated in this study are presumably linked to the glacially reworked, smectite-free material brought by BRS and deposited in the area of SNS during the Early Pleistocene. Although I-S mixed-layer minerals are not uncommon for Quaternary deposits of cold latitudinal zones, their peculiar distribution in the analyzed sedimentary succession and the

https://doi.org/10.1346/000986016820500438 Published online by Cambridge University Press

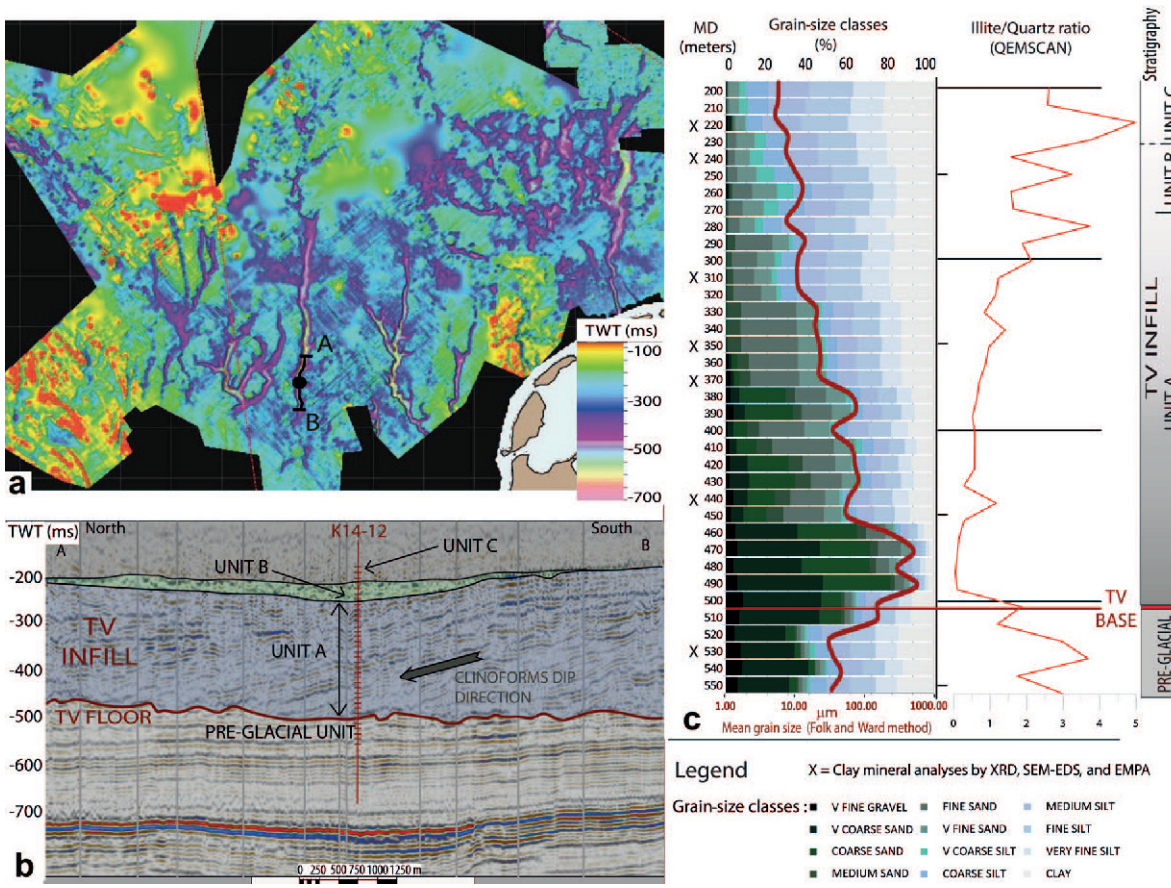

Figure 2. (a) Map showing the depths (expressed in two-way time) of the glacial unconformity mapped on 3D high-resolution seismic data by Moreau *et al.* (2012). A large number of incisions (TVs) are evident in this reconstruction. The location of the seismic reflection profile is indicated by a black line and the black dot shows the location of borehole K14-12. (b) N–S oriented seismic section showing the stratigraphic architecture. The TV base is highlighted in red, separating the pre-glacial deposits from the overlying TV infill. The main infill of the TV is defined by a thick interval of northward-dipping reflectors (Unit A), overlain by a thin interval of horizontal reflectors in a restricted area (Unit B), and a widespread interval characterized by a chaotic seismic facies (Unit C). Well K14-12 is identified by a vertical red line. A constant velocity of 1900 m/s was used for time-depth conversion (Benvenuti and Moscariello, 2016). (c) Histogram showing the grain-size distributions with the green line indicating mean values (Folk and Ward, 1957) for 36 sediment samples (from ditch cuttings). The illite/quartz ratio was calculated from QEMSCAN® (FEI QEMSCAN® Quanta 650F, Oregon, USA) data. The stratigraphic succession of the TV infill and post-glacial deposits is modified after Benvenuti and Moscariello (2016).

distinct mineralogical and geochemical characteristics put forth a possibility of diagenetic *in situ* origin of smectite mixed layering (*i.e.* smectitization of illite). The deep sediment burial usually held responsible for I-S formation through the illitization of smectite (Chamley, 1989) cannot explain the origin of I-S from the sediments studied because of the shallow burial history of the deposits which have never experienced a burial depth >550 m. The purpose of this study, therefore, was to frame and test the hypothesis that reaction of detrital illite with cold freshwater in a glaciolacustrine meltwater paleoenvironment produced early diagenetic mixed-layer I-S. Mineral transformations of this type are usually referred to as 'degradation' and are characteristic of continental weathering (Thorez, 1989), rarely taking place during sedimentation and diagenesis (Millot, 1971). In the latter case, the sediment must have been exposed to percolating solution able to degrade clay minerals, which is the process reported only rarely in the literature (Smoot, 1960). This paper provides the first evidence of early diagenetic transformation of illite into I-S in the Quaternary sediments of the North Sea, within the peculiar glaciogenic microenvironment of TVs and where meltwater played a role of degrading fluids. Clay mineralogy thus provided new constraints on the mechanism of TV formation and sediment filling, which may be of global importance as TVs are still being formed at the margins of continental ice sheets, and the fine fraction of their sedimentary infill is seriously under researched (*e.g.* Kehew *et al.*, 2012). The freshwater hydrologic system advocated in the present study as being indispensable for illite transfor-

https://doi.org/10.1346/000986016820500438 Published online by Cambridge University Press

mation into intermediate I-S is discussed further in light of the debate on a Pleistocene proglacial lake. Such a lake has been suggested previously to exist at the southern margin of the ice-sheet in an area comprising the Benelux countries and the uncovered part of the SNS (Figure 1; *e.g.* Gibbard, 2007; Gupta *et al.*, 2007; Murton and Murton, 2012).

STRATIGRAPHIC CONTEXT AND DESCRIPTION OF THE MATERIAL SAMPLED

The Elsterian TV investigated in the present study represents the largest such feature currently known in the SNS (Moreau *et al.*, 2012). The valley is an elongated north–south depression, 100 km long, 2–3 km wide, and up to 500 m deep (Benvenuti and Moscariello, 2016). The TV is filled with a thick succession of deposits that appear as three different units on seismic sections: a lower northward dipping clinoform-dominated unit (Unit A), an upper horizontal layered unit (Unit B), and a unit characterized by chaotic seismic facies (Unit C) (Figure 2b; Benvenuti and Moscariello, 2016). Sediment samples (ditch cuttings) from the borehole K14-12 located in the K block of the Dutch offshore were provided by Nederlandse Aardolie Maatschappij (Shell) (Figure 2). For the purpose of this research, 36 sediment samples were collected at 10-m intervals. Drilling mud consisted of seawater bentonite and carboxymethylcellulose (CMC) mud (Shell, 1993), with minimal influence on sample mineralogy as indicated by the almost complete absence of discrete smectite agglomerations.

Samples cover a measured depth (MD) interval along the borehole of 550 to 200 m and are named after their position along the borehole. Those from between 550 and 500 m define the pre-glacial sediments below the TV floor (Benvenuti and Moscariello, 2016). In the study area, Harding (2015) showed the presence of a thick package of sediments dating from Lower Early Pleistocene at the depths investigated in the present research. The TV floor is identified at 500 m. Samples from the 490–280 m range represent the northward-dipping clinoform unit (Unit A). Samples from between 270 and 240 m are from the unit dominated by horizontal layers (Unit B). Material from 230 m samples the chaotic unit that is poorly characterized, given the inadequate seismic data quality at shallow intervals (Unit C). Investigation by QEMSCAN® (FEI QEMSCAN® Quanta 650F, Oregon, USA) was performed on the entire range of samples, while seven samples were selected to study the clay fraction in detail.

ANALYTICAL METHODS

Grain-size analysis

All 36 sediment cutting samples were sieved using a two-step sieving procedure. First, wet sieving was performed on 30 g of dry, loose material. Sieves ranged from 0.063 to 2 mm on a φ scale-based succession. Following complete drying, each sample and every size class of the material were weighed. The material finer than 0.063 mm was analyzed using a laser particle size analyzer CILAS 1180 (CILAS, Orléans, France) installed at the Department of Earth Sciences (University of Geneva, Switzerland). Coarse particles were measured using a real-time fast Fourier transform of the image obtained with a charge-coupled device camera equipped with a digital processing unit. The results for particle sizes were recovered in vol.% and were later converted to grams to conform to the overall dataset obtained by manual sieving. The data were treated with the GRADSTAT software (Blott and Pye, 2001) yielding the results displayed as percentages of the respective grain-size classes and as averages (Folk and Ward, 1957).

QEMSCAN® and SEM study of clay morphology

In order to produce thin sections used for the microbeam investigations (QEMSCAN®, scanning electron microscopy-energy dispersive spectroscopy (SEM-EDS), electron microprobe analysis (EMPA)), the rock chips were mounted on the glass substrate using ARA XW 396 epoxy resin combined with the ARA XW 397 hardener, at a weight ratio of 10:3. The injection of resin was completed under vacuum and thin sections produced were dried for 12 h at 50ºC.

Automated mineral and textural characterization was performed using a QEMSCAN® facility. This system featured the field emission gun (FEG) electron source and is installed at the Department of Earth Sciences (University of Geneva, Switzerland). Mineral-phase identification relies on the combination of back-scattered electron (BSE) contrast and EDS spectra giving information on the elemental composition (Gottlieb *et al.*, 2000). Individual X-ray spectra were compared to a library of known spectra and a mineral name was assigned to each individual acquisition point. The X-ray EDS spectra library, initially provided by the manufacturer, has been developed further in-house using a variety of natural standards. Measurements were performed on carbon-coated thin sections that were minimally polished in order to avoid a clay-fraction loss. Analytical conditions included a high vacuum and an acceleration voltage of 15 kV with probe current of 10 nA. X-ray acquisition time was 10 ms per pixel using a point-spacing of 2.5 μm. Up to 122 individual fields of view were measured in each sample, with 1.5 mm per single field.

Gold-coated thin sections were used for SEM investigations. Crystal morphology, shapes, and mineral agglomerations were studied by high-magnification back-scattered electron (BSE) and secondary electron (SE) imaging using the QEMSCAN® facility operated in SEM mode under high vacuum. A variety of acceleration

https://doi.org/10.1346/000986016820500438 Published online by Cambridge University Press

voltages and beam-size conditions were employed to ensure the best imaging conditions.

XRD mineralogy

X-ray powder diffraction was performed on whole-rock samples, as well as the clay fraction. Sample preparation initially included material powdering in an agate mortar prior to whole-rock measurements. Seven representative samples, covering the whole stratigraphic section investigated, were chosen for further investigations of the clay-mineral fraction (Figure 2c). To prevent possible mixing of detrital with authigenic clays, the samples were not powdered but disaggregated gently. The clay fraction was separated from the crushed material by centrifugation, which first involved the removal of organic matter using 10 wt.% H_2O_2 for at least 24 h. Na-metaphosphate was added to disperse the clays. Further disaggregation was accomplished in an ultrasonic bath. To ensure a uniform cation exchange, clay fractions separated by centrifugation were saturated by Mg using a solution of 10 mL of ~4 M $MgCl_2$. Suspensions were washed and centrifuged with distilled water at least three times to minimize the free-ion content. The oriented mounts were prepared using a Millipore membrane filter and a vacuum filtration device. After the clay suspension was drawn onto the filter, it was left to dry at 50ºC prior to the transfer to porous ceramic tiles. The thickness of such prepared mounts exceeded 50 μm, which is required for semi-quantitative determination of the clay-mineral content (*e.g.* 'infinite thickness' of Moore and Reynolds, 1997). The rest of the clay-fraction material was used for laser particle-size analysis using the CILAS 1180 device as described above.

The measurements were undertaken in air-dried (AD) conditions, after ethylene-glycol (EG) saturation, and after heating for 1 h at 300ºC. A Bruker D8 Advance diffractometer (Bruker AXS GmbH, Karlsruhe, Germany) was used for XRD analyses. This instrument features a horizontal goniometer axis and synchronized rotation of both the X-ray source and the detector arms. The sizes of the divergent and the receiving slits were 1º and 0.1 mm, respectively. Measurement parameters consisted of a continuous scan in the Bragg-Brentano geometry using CuKα radiation (45 kV and 44 mA) with a curved-graphite monochromator. At a counting time of 370 s per 0.012º2θ, sample mounts were scanned from 3 to 70 and from 3 to 30º2θ for the whole rock and the clay fraction, respectively.

Electron microprobe analyses

Electron microprobe analyses and elemental X-ray study were carried out using a JEOL JXA 8200 Superprobe (JEOL Ltd., Akishima, Japan) with a wavelength/energy dispersive combined microanalyzer. Operating parameters included an accelerating voltage of 20 kV, a 20 nA beam current, and a 1 μm beam size. Counting times of 20 s on peak and 10 s on background on both sides of the peak were used for all elements. Limits of detection (LOD) were calculated as the minimum concentration required to produce count rates three times higher than the square root of the background (3σ; 99 wt.% degree of confidence at the lowest detection limit). Concentrations below the LOD are reported as not detected. Raw data were corrected for matrix effects using the PAP algorithm implemented by JEOL (Pouchou and Pichoir, 1984, 1985). Natural minerals, oxides (corundum, spinel, hematite, and rutile), and silicates (albite, orthoclase, anorthite, and wollastonite) were used for calibration. Mineral formulae were calculated using a software package designed by H-P. Meyer (University of Heidelberg, Germany). For the calculation of illite and mica formulae, all Fe was assumed to be Fe(III). Iron, Mg, and Ti were assumed to be octahedral, while Al was assumed to be tetrahedral up to Si + Al = 4 atoms per 11 oxygens, with the remaining Al assigned to octahedral sites. For mixed-layer minerals containing smectite, the totals of measured elements ranged between 70.01 and 82.92 wt.%, thus reflecting (1) the difference in smectite component abundances, (2) large amounts of water in the smectite component, and (3) the potential porosity between clay particles.

Interpretation and modeling of XRD patterns

The mineral phases were identified using the Powder Diffraction File (1996) data system and the *Panalytical*© *HighScore Plus* (v. 3.0e) program package (PANalytical, Almelo, The Netherlands). X-ray diffraction patterns of clay minerals were examined using methods described by Moore and Reynolds (1997) and Środoń (2006). For chlorite-mineral interpretation, the recommendations of Lagaly *et al.* (2006) and Meunier (2007) were followed. Illite crystallinity values, known better in recent years as the 'Kübler index' (KI: Kubler, 1964; Guggenheim *et al.*, 2002) and defined by the width of the illite 001 peak measured at half of the peak height above the background (Eberl and Velde, 1989), were measured using the Panalytical© X'pert data viewer. Expressed as ºΔ2θ, KI values were used to characterize the environment of illite formation, taking into account that diagenetic illite has KI values of >0.42ºΔ2θ, whereas the range of KI values from 0.30 to 0.42ºΔ2θ corresponds to low metamorphic anchizone, from 0.25 to 0.30ºΔ2θ is the high anchizone and KI <0.25ºΔ2θ defines the metamorphic epizone (*e.g.* Kemp and Merriman, 2009). The calibration of KI values was carried out using the international standards provided by Warr and Rice (1994). Characterizing mixed layering only by analyzing the 001/002 and 002/003 I-S peak positions was practically impossible given the fact that the samples analyzed consisted of detrital illite and I-S mixed-layer minerals both rich and poor in illite (Moore and Reynolds, 1997). To characterize the mixed-layer clay

https://doi.org/10.1346/000986016820500438 Published online by Cambridge University Press

minerals, XRD clay fraction patterns were, therefore, modeled using *Sybilla*© software (property of Chevron™, San Ramon, California, USA) based on the formalism of Drits and Sakharov (1976). The modeling included a trial-and-error procedure that provided optimal clay-mineral structural and probability parameters to obtain the best fit between experimental and calculated patterns and of the intensities of the 00*l* reflections for each of the clay phases present. For mixed-layer minerals, the number, nature, and stacking sequence of different compositional layers were taken as modifiable values (*e.g.* Uzarowicz *et al.*, 2012).

To produce the experimental spectra, three discrete phases were introduced (illite, chlorite, and kaolinite). R3 I-S, a mixed-layer illite-smectite with long-range ordering (Reichweite >1), was introduced to accommodate the 001 peak asymmetry of illite at lower 2θ values. Larger background values between the 001 peaks of chlorite and illite were modeled by addition of low ordered (Reichweite = 0) R0 I-S and R0 I-SS. The second S denotes a multiple type of smectite component differing from the preceding one in terms of charge and, therefore, in terms of *d* spacing. In other words, expandable layers in R0 I-S are bi-hydrated and in R0 I-SS they are mono- and bi-hydrated (*e.g.* Suquet *et al.*, 1975; Ferrage *et al.*, 2005). The hydration properties of the smectite component are normally related to their charge deficit (Drits, 2003). Thus, in R0 I-SSS introduced to mimic an intensity increase reported at ~5º2θ, the third type of smectite layer is an intermediate between smectite and vermiculite with a slightly contacted smectite-type layer with a default *d* spacing of 14 Å.

An additional mixed-layer phase, kaolinite-smectite (K-S), was used also, fitting the low-angle shoulder at the kaolinite basal diffraction peak. The R0 variety was used because most documented K-S occurrences were randomly interstratified (*e.g.* Dudek *et al.*, 2006). Modeling parameters of mixed-layer minerals consisted of (1) the extent of preferred orientation of particles on the mounted X-ray slides (σ*), (2) coherent scattering domain sizes (CSDS) expressed in number of layers, and (3) the amounts of smectite component in mixed-layer phases (Table 1). The relative clay mineral content was determined using the integrated peak areas of illite (002), kaolinite (002), and chlorite (003) weighted by appropriate mineral reference intensities and normalized (Moore and Reynolds, 1997). The relative abundance of clay minerals was, therefore, refined using *Sybilla*© modeling, allowing the amounts of smectite layers present in mixed-layer clay phases to be estimated.

Deconvolution of the air-dried XRD patterns was performed using *DecompXR* software (Lanson, 1993). The area modeled ranged from 5 to 10º2θ where, depending on the composition of mixed-layer I-S, its first basal diffraction peak is located. Having subtracted the background, experimental patterns were fitted with six Gaussian elementary curves representing mineral compounds used for *Sybilla* modeling (illite, chlorite, R3 I-S, R0 I-S, R0 I-SS, and R0 I-SSS). All the compounds met the criteria of Lanson and Besson (1992) requiring the elemental curves to have a minimum peak position and a width difference of 0.3 and 0.2º2θ, respectively.

Statistical analyses

Multivariate statistical analysis, specifically principal component analysis (PCA), was performed on seven samples to identify the principal components that control variations in mineralogical abundances and the relationship between mineral phases and grain-size classes. The analysis was conducted on mineral compositional data of

Table 1. *Sybilla*© modeling parameters of mixed-layer phases (R0 I-S, R0 I-SS, R3 I-S, and R0 K-S).

Samples/ Phase parameters	220	240	310	350	370	440	530
σ* (R0 I-S)	12º	12º	12º	12º	11º	11º	11º
CSDS (R0 I-S)	7	7	7	7	7	7	7
Sme (R0 I-S)	20	20	26	31	28	28	21
σ* (R0 I-SS)	12º	12º	12º	12º	12º	12º	12º
CSDS (R0 I-SS)	5	5	5	5	5	5	5
Sme (R0 I-SS)	81	81	81	92	94	82	75
σ* (R3 I-S)	12º	12º	12º	12º	12º	12º	12º
CSDS (R3 I-S)	12	15	15	15	15	15	15
Sme (R3 I-S)	5	5	5	5	9	9	13
σ* (R0 K-S)	10º	10º	10º	10º	10º	10º	10º
CSDS (R0 K-S)	7	7	7	7	7	7	7
Sme (R0 K-S)	2	2	2	2	6	6	1

σ* – preferential particle orientation parameter (recommendation of Moore and Reynolds (1997) is to set σ* around 12º for all clay minerals during spectra modeling); CSDS – coherent scattering domain sizes expressed in number of layers; Sme – smectite content in the respective mixed-layer mineral (in wt.%); I-S and K-S – mixed-layer illite-smectite and kaolinite-smectite, respectively; R – Reichweite (measure of order); Parameters of R0 I-SS not given as this entry is used to mimic I-S superstructure 001* diffraction peak partly masked by primary radiation.

https://doi.org/10.1346/000986016820500438 Published online by Cambridge University Press

the fine fraction as determined after the modeling of the XRD patterns. The centered log-ratio transformation (Aitchinson, 1982) was applied to the compositional data in order to remove the non-negativity and constant-sum constraints typical of compositional variables. The PCA analysis was conducted by '*R*' software ("R core team," New Zealand) using the package *FactoMineR* (Lê *et al.*, 2008). Grain-size data, expressed in volume of material per grain-size class, were used in line with the mineral composition data as quantitative supplementary variables.

RESULTS

Grain-size and bulk-rock mineralogy

The lower parts of the Elsterian TV analyzed (Unit A, Figure 2c) contain sediments dominated by medium to coarse sand with the mean (after Folk and Ward, 1957) grain size of ~500 μm. Higher in the succession, the grain size became progressively finer, reaching 20 wt.% clay in the upper portions of Unit A (TV infill), as well as Units B and C. In Units B and C the abundance of sand was <10 wt.%, with a mean particle size of ~10 μm and less. The pre-glacial sediments below the Elsterian TV are characterized by a clear bimodal character having practically equal amounts of gravel and sandy grains *vs.* clay and fine silt particles. The mean grain size was in the medium silt range (~50 μm), although the bimodal size distribution means that this mean is not represented amply in the sediments.

The modal mineralogy was clearly controlled by variations in the grain size up the stratigraphical section (Figure 2c). Quartz is most abundant in the lower portions of Unit A, where the sediment is coarsest. In contrast, in the fine-grained portion of the section (*i.e.* the uppermost stratigraphic interval) the highly crystalline illite was the dominant phase; elsewhere it was the second most abundant component. Particularly illustrative is the illite/quartz ratio, being practically inversely proportional to the mean grain-size curve (Figure 2c), thus suggesting that quartz and illite dominated the coarse and fine fractions, respectively. Feldspars, generally albitic, made up <10 wt.%. Biotite and muscovite, up to several mm in grain size, are widespread but occur in relatively small amounts (~3 wt.%). The carbonate minerals, calcite and aragonite, were abundant in the coarse fraction, occurring exclusively as bioclasts. Agglomerates of detrital grains coated by a pyritic and/or sideritic matrix were abundant in the pre-glacial deposits, while they were less abundant in the TV infill, and increased in abundance in the Units B and C. The coarse size of bioclasts and diagenetic minerals caused a bimodality of the grain-size curve of the pre-glacial deposits as well as in some samples of Units B and C (Figure 2c). Clay minerals other than illite (*i.e.* kaolinite, chlorite) were detected by QEMSCAN® and XRD whole-rock measurements only in small amounts (~0.5–1 wt.%, 2–3 wt.%, respectively; Table 2). Discrete smectite was not detected by XRD measurements, while in the QEMSCAN® analyses, smectite occurred in very small amounts (<0.2 wt.%, Table 2).

Clay mineralogy and SEM characterization of clayey particles

An assemblage consisting of illite, illite-smectite, kaolinite, and chlorite characterized the clay fraction (Figure 3). The summed abundances of illite and various mixed-layer illite-smectites varied between 63 wt.% in pre-glacial deposits (sample 530) and 80 wt.% in Unit C (sample 220, Table 3). The amounts of chlorite and kaolinite (including K-S) were between 5 and 8 wt.% and between 15 and 30 wt.%, respectively (Table 3). The abundance of kaolinite was inversely proportional to the amount of illite and illitic minerals, with the largest amount of kaolinite and the smallest amount of illite and illitic minerals recorded in pre-glacial deposits, whereas in the post-glacial layers the ratio was the inverse (Table 3). Small percentages of non-clay minerals (quartz and feldspar) were also detected in all the samples analyzed (Figure 3), but these were not taken into account during quantification. Based on the analysis of XRD patterns, the results of spectral modeling, and the study of particle morphologies, the following detailed characterization of clay minerals was prepared.

Illite. Illite was defined by the sequence of basal 00l diffraction peaks that were unaffected by glycolation (Figure 3, EG curves). Relying on the profile fitting and deconvolution (Figures 4–5), illite consisted of two non-expandable phases between d_{001} 9.96–10.01 (illite *sensu stricto*) and d_{001} 10.08–10.14 Å (R3 I-S), with <5 and 13 wt.% smectite layers, respectively (Table 1). In general, the 001 peaks of illite are relatively broad with illite KI values ranging from 0.415 (sample 240) to 0.341°Δ2θ (sample 310). The SEM-EDS investigation revealed illite forming irregular flake-like platelets oriented parallel to each other (Figure 6a). Illite occurs sparsely in a rod-like form (Figure 6b). In either case, relations between XRD mineralogy and particle grain sizes revealed the size of illite particles to be in the range of several microns (Figure 7a**)**. Somewhat larger particles (~10–15 μm) were probably muscovite (Figure 6a) or biotite (Figure 6b).

Mixed-layer illite-smectite. Expandable interstratifications of illite and smectite were identified as mixed-layer I-S and were first identified visually using the criteria of Reynolds and Hower (1970) due to a broad diffraction peak at ~17 Å appearing in EG samples (Figure 3). More information about the nature of I-S was provided by pattern fitting which revealed the presence of two disordered smectite-rich mixed-layer I-S (R0 I-S, R0 I-SS, Table 1) which accompanied a disordered R0 K-S and ordered R3 I-S (Table 1). These four mixed-layer

https://doi.org/10.1346/000986016820500438 Published online by Cambridge University Press

Table 2. Modal mineralogy (wt.%) based on QEMSCAN® and XRD whole-rock measurements.

Sample	Qtz	Pl	Kfs	Cal/ Arg	Dol	Ms	Bt	Ill	Sme	Kln	Chl	Sd	Py	HMs	Un- class.	I/Qtz
200	21.18	3.64	1.35	3.98	1.18	1.67	4.09	55.47	0.32	1.08	1.90	0.26	0.63	0.34	2.90	2.62
210	21.68	3.54	1.58	3.63	1.14	1.60	5.13	56.04	0.27	0.95	2.00	0.08	0.53	0.39	1.44	2.58
220	12.13	2.37	0.74	3.80	0.44	1.65	6.16	60.56	0.21	1.02	2.15	0.11	5.17	0.24	3.24	4.99
230	15.53	2.76	1.24	0.92	0.36	1.08	10.71	58.80	0.77	0.82	4.13	0.02	0.78	0.25	1.83	3.78
240	30.13	5.06	3.27	2.82	1.27	1.34	2.21	47.66	0.14	0.85	1.02	0.09	0.87	0.41	2.86	1.58
250	19.40	3.69	1.94	1.53	0.63	0.88	3.59	63.01	0.20	0.67	1.73	0.04	0.62	0.30	1.78	3.24
260	31.54	3.76	2.70	1.28	0.64	0.81	4.80	49.71	0.16	0.59	1.43	0.02	0.70	0.38	1.46	1.57
270	29.59	4.71	2.46	1.71	0.81	1.16	4.88	48.45	0.30	0.80	2.21	0.05	0.89	0.46	1.53	1.63
280	17.19	2.66	1.45	0.96	0.36	0.91	6.92	64.13	0.26	0.68	2.06	0.02	0.90	0.21	1.31	3.73
290	28.05	3.51	2.34	1.61	0.68	1.10	4.50	52.85	0.25	0.83	2.20	0.06	0.69	0.35	0.97	1.88
300	25.98	3.52	1.81	1.48	0.48	0.87	5.94	55.33	0.17	0.54	1.22	0.04	0.69	0.29	1.64	2.13
310	36.99	3.01	2.63	1.72	0.68	0.90	2.49	45.46	0.09	0.60	0.68	0.59	0.75	0.26	3.14	1.23
320	37.40	3.99	2.78	1.85	0.64	0.89	3.19	42.79	0.14	0.49	0.97	0.05	0.81	0.26	3.74	1.14
330	45.52	3.83	3.39	2.19	0.56	0.57	1.38	37.97	0.09	0.40	0.82	0.03	0.77	0.29	2.18	0.83
340	34.97	3.29	2.78	1.35	0.53	0.70	1.98	49.15	0.17	0.62	1.57	0.07	0.54	0.25	2.03	1.40
350	42.76	3.73	3.54	1.51	0.61	0.72	2.07	41.03	0.11	0.49	0.91	0.05	0.64	0.31	1.52	0.96
360	44.18	4.50	3.59	1.72	0.69	0.82	1.64	38.38	0.12	0.49	1.11	0.07	1.16	0.43	1.13	0.86
370	48.31	4.19	3.64	1.51	0.54	0.69	1.52	33.82	0.11	0.46	0.99	0.06	1.87	0.34	1.94	0.70
380	44.74	4.07	3.72	6.49	0.51	0.73	1.57	28.33	0.09	0.40	0.70	0.05	6.09	0.34	2.16	0.63
390	47.38	3.56	3.10	8.24	0.48	0.55	1.21	24.25	0.08	0.32	0.46	0.05	8.69	0.30	1.33	0.51
400	48.41	3.68	3.59	9.92	0.53	0.54	0.93	28.06	0.08	0.40	0.75	0.52	0.86	0.33	1.41	0.58
410	48.79	4.64	3.26	7.25	0.50	0.72	1.99	28.11	0.14	0.36	0.61	0.23	1.16	0.32	1.92	0.57
420	47.00	3.07	3.38	9.51	0.39	0.54	1.74	26.80	0.11	0.37	0.55	0.04	1.74	2.91	1.84	0.57
430	60.82	3.12	3.41	11.83	0.38	0.47	0.77	16.68	0.08	0.21	0.34	0.02	0.76	0.24	0.88	0.27
440	35.93	2.81	2.12	7.98	0.48	0.78	3.18	41.78	0.23	0.47	1.67	0.05	1.22	0.25	1.02	1.16
450	52.37	2.11	1.98	20.36	0.30	0.32	0.63	14.91	0.08	0.20	0.28	0.02	3.91	0.20	2.34	0.28
460	55.29	1.78	2.11	26.27	0.25	0.35	0.37	7.73	0.03	0.22	0.38	0.11	4.28	0.28	0.54	0.14
470	42.30	2.21	5.04	43.35	0.11	0.14	0.19	3.82	0.02	0.09	0.19	0.02	0.62	0.16	1.76	0.09
480	64.10	1.54	1.36	27.14	0.20	0.21	0.17	2.69	0.03	0.13	0.18	0.02	1.00	0.20	1.02	0.04
490	60.16	3.95	7.20	19.12	0.57	0.35	0.34	5.24	0.03	0.15	0.45	0.03	0.94	0.36	1.10	0.08
500	26.35	1.77	1.03	14.74	0.28	0.49	2.90	48.92	0.14	0.51	1.00	0.08	0.77	0.16	0.84	1.85
510	27.14	1.76	5.14	23.29	0.31	0.43	0.90	32.54	0.06	0.67	0.52	2.01	2.47	0.13	2.63	1.20
520	17.77	1.68	1.02	12.59	0.87	0.49	0.53	53.01	0.20	2.08	0.66	0.06	3.47	0.16	5.39	2.98
530	15.07	1.33	0.83	4.97	0.17	0.60	3.41	55.79	0.14	0.82	0.97	2.28	8.67	0.13	4.83	3.70
540	23.57	1.47	1.35	21.27	1.78	0.57	2.04	41.40	0.20	0.85	0.98	0.05	1.55	0.62	2.31	1.75
550	15.18	1.25	0.57	20.54	1.03	0.53	2.05	45.25	0.17	0.88	1.01	0.04	6.96	0.14	4.39	2.98

Qtz: quartz; Pl: plagioclase; Kfs: K-feldspar; Cal/Arg: calcite/aragonite; Dol: dolomite; Ms: muscovite; Bt: biotite; Ill: illite; Sme: smectite; Kln: kaolinite; Chl: chlorite; Sd: siderite; Py: pyrite; HMs: transparent heavy minerals (hornblende, epidote, garnet); Unclass.: QEMSCAN® unclassified data. Mineral abbreviations after Kretz (1983) and Whitney and Evans (2010).

Table 3. Relative clay mineral abundances in the samples analyzed (wt.%).

Sample	Ill (s.s.)	Kln	Chl	R3 I-S	R0 I-S	R0 I-SS	R0 I-SSS	R0 K-S	Sme_{TOT}
220	18	8	8	34	20	3	2	7	8
240	23	8	7	18	23	2	4	15	11
310	15	7	5	19	35	4	4	11	16
350	14	9	5	22	29	3	8	10	20
370	17	9	6	17	29	3	6	13	18
440	19	10	5	19	25	7	5	10	17
530	13	10	5	26	20	4	2	20	12

I-S and K-S – mixed-layer illite-smectite and kaolinite-smectite, respectively; R – Reichweite (measure of order); Sme_{TOT} – total smectite content in all I-S mixed-layer phases containing smectite, only R0 I-SSS not considered; Ill (s.s.): illite *sensu stricto*; Kln: kaolinite; Chl-chlorite. Mineral abbreviations after Kretz (1983) and Whitney and Evans (2010).

https://doi.org/10.1346/000986016820500438 Published online by Cambridge University Press

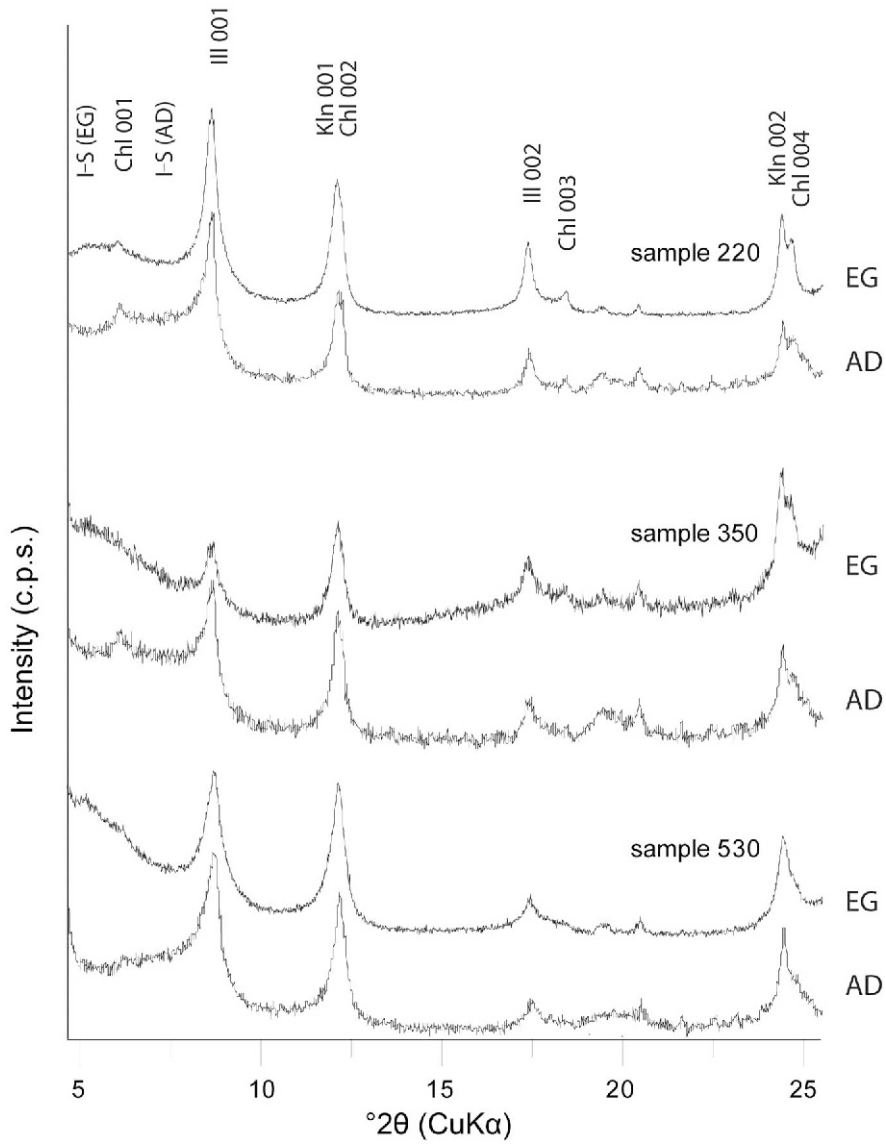

Figure 3. Mineral composition of the clay factions (<0.2 μm) analyzed, shown for three representative samples. EG = treatment with ethylene-glycol; AD = air-dried samples. Measurements after heating are not shown (see text). Mineral symbols: I-S (illite-smectite), Chl (chlorite), Ill (illite), and Kln (kaolinite).

minerals fitted the experimental spectra well (Figure 4). The XRD pattern deconvolution preformed after Lanson and Velde (1992) on asymmetric 10 Å bands showed R0 I-S at d_{001} 10.77−10.81 Å and R0 I-SS at d_{001} 13.72−13.80 Å (Figure 5). Both disordered I-S had wide peaks indicating small crystallite thicknesses that continued to diminish as the amount of smectite layers increased. The smectite content was estimated to be between 20−31 and 75−94 wt.% for R0 I-S and R0 I-SS, respectively (Table 1). The curve attributed to R0 I-SSS has no physical meaning but it was introduced for curve-fitting purposes in the area of ~5º2θ where greater intensities were observed probably due to the effects of the incident X-ray beam (*e.g.* Allmann, 2003).

The SEM-EDS showed I-S particles with a flaky morphology that is analogous to that of presumably discrete illite with comparatively smaller particle sizes in the micron range (Figures 6a,b, 7b). Occasionally, I-S is reported forming coarser agglomerates which are several microns in size (Figure 6c). Mixed-layer phases formed the largest portion of the sample matrix (Figure 6b). Taking into account the Ca content, as well as the octahedral Fe/Mg and in particular tetrahedral Al/Si ratios, the SEM-EDS investigations allowed a quick identification of disordered (smectite-rich) I-S varieties (Welton, 1984), which was further corroborated by EMPA measurements on several representative sample portions.

https://doi.org/10.1346/000986016820500438 Published online by Cambridge University Press

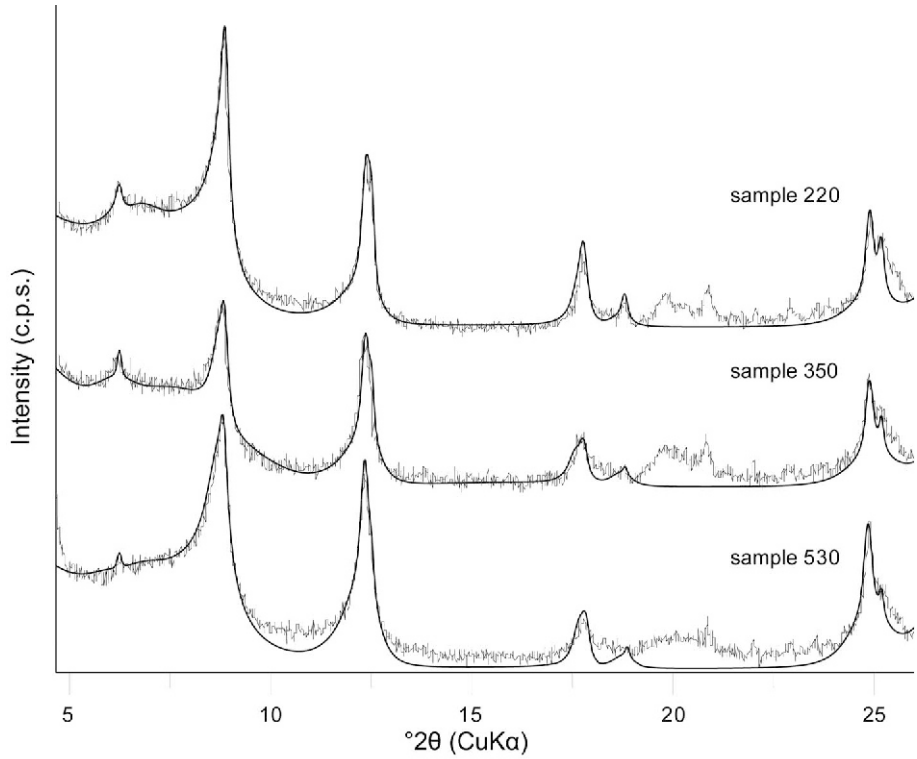

Figure 4. Comparison between experimental (zigzag line) and calculated (continuous line) XRD patterns for three representative measurements on clay fractions (air-dried).

Chlorite. Despite the fact that the basal peaks of chlorite overlapped partly with kaolinite, chlorite was defined by its d_{002} and d_{004} diffraction peaks at 7.12 and 3.55 Å, respectively (Figures 3–4). Its weak, odd-order diffraction peaks were highly pronounced when the 001 diffraction peak was strongly attenuated. This indicates large Fe abundances in the chlorite structure (Moore and Reynolds, 1997). Using the intensity ratios $I(003)/I(005)$ (Brown and Brindley, 1980) and profile fitting, the total Fe content in chlorite was found to be ~2.34 a.p.f.u., which corresponds well with the Fe concentration in chlorite determined by EMPA (2.19 a.p.f.u., Table 4). A heat treatment at 300ºC showed no evidence that a partly expandable vermiculite-type phase of 14 Å was present. In SEM-EDS, chlorite appeared either as relatively coarse detrital grains (up to 50 μm in size, Figure 6b) or replacing crystallites of biotite (Figure 6d). No significant differences in the crystal chemistry between the two chlorite habits were documented.

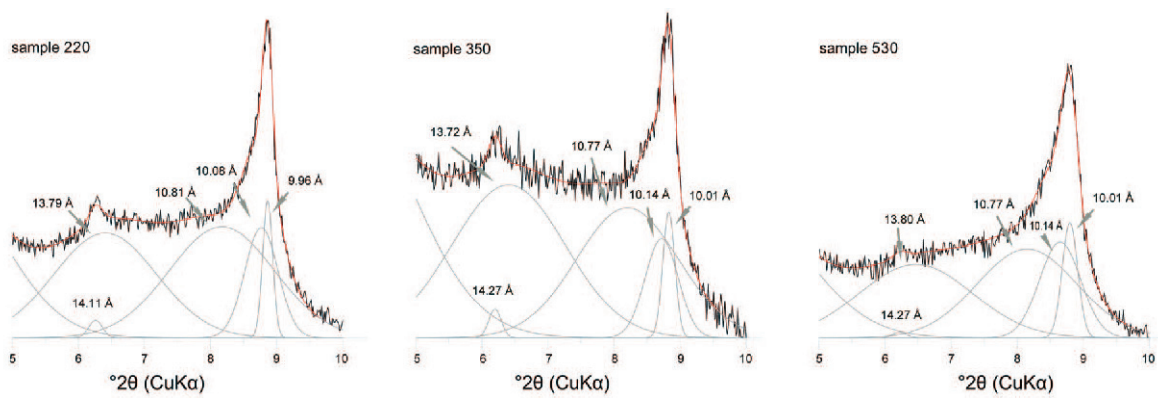

Figure 5. Deconvolution of XRD patterns of the clay fraction (air-dried) for three representative samples. The experimental XRD patterns are zigzag and black, the best fits are continuous and red (see online version for color), while elementary Gaussian curves are continuous and light gray.

https://doi.org/10.1346/000986016820500438 Published online by Cambridge University Press

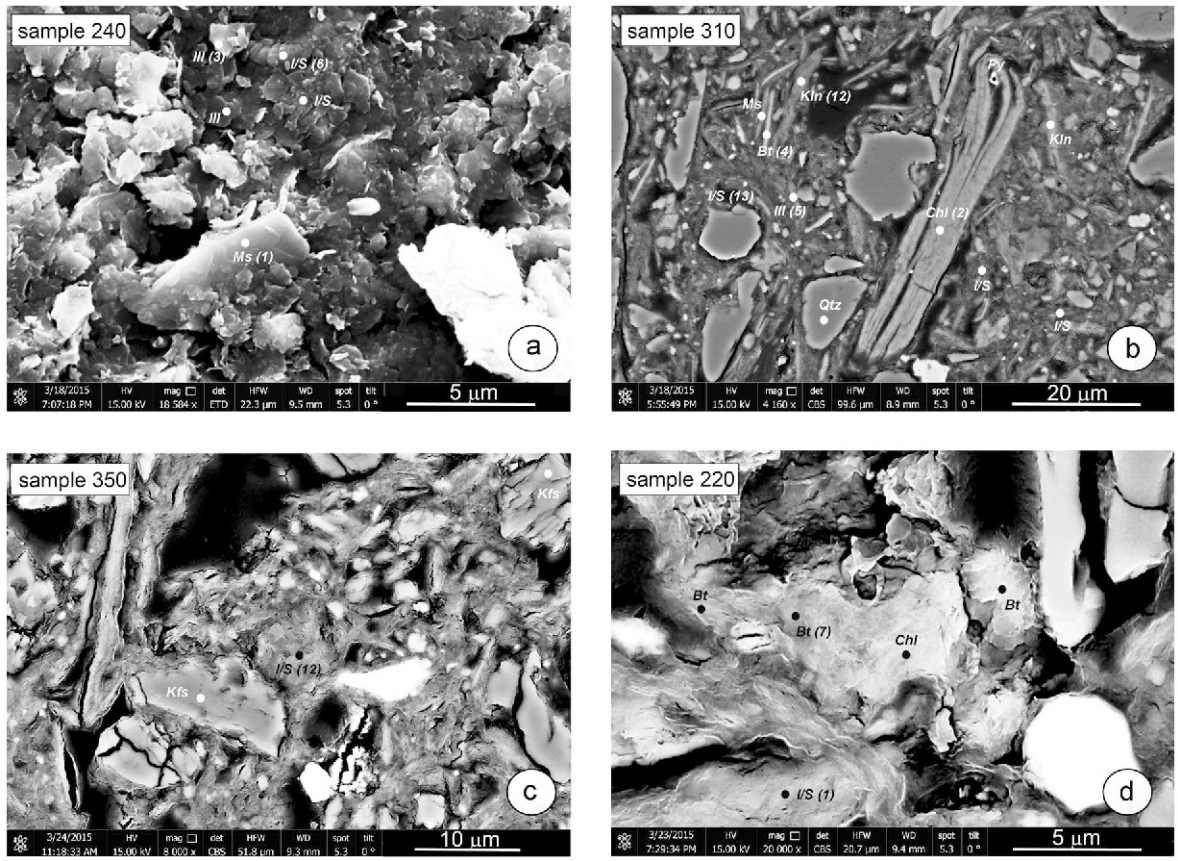

Figure 6. SEM images of sediment samples showing: (a) illite and I-S crystals forming irregular flake-like platelets oriented parallel to each other; (b) rod-like illite and relatively coarse chlorite and kaolinite agglomerates; (c) agglomerates of smectite-rich interlayered I-S; and (d) chlorite mineralization growing at the expenses of biotite. The points and digits placed on some of the minerals stand for microprobe analyses and their corresponding numbers. The representative microprobe data are provided in Table 4.

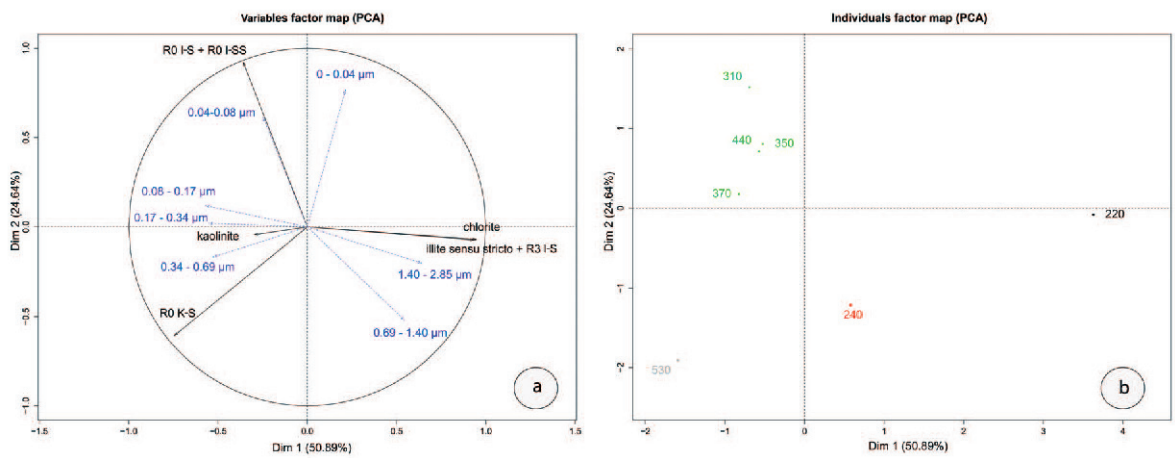

Figure 7. (a) The variable-projection image illustrating the correlation of smectite-rich phases with the finest grain fraction, and conversely the association of chlorite and illite with the coarsest grain fraction. (b) The principal component biplot (Dim 1 and Dim 2) based on the fine-fraction mineralogical composition and grain-size classes, showing sample groupings according to their stratigraphic positions.

https://doi.org/10.1346/000986016820500438 Published online by Cambridge University Press

Table 4. Selected microprobe analyses and formulae of illite, chlorite, illite-smectite, muscovite, and biotite.

	Illite				Illite-Smectite								Kaolinite		Chlorite	Muscovite		Biotite	
Sample	240	410	310	220	240	370	350	530	310	240	410	530	310	530	310	240	410	310	220
Anal. No.	3	8	5	2	6	2	12	2	13	15	12	5	12	13	2	1	10	4	7
SiO_2	48.63	47.79	46.63	47.49	44.97	45.53	39.72	41.28	38.31	45.30	39.22	41.12	42.41	45.35	26.80	47.29	48.39	48.17	45.14
TiO_2	0.29	0.77	0.21	0.45	0.64	0.36	0.23	0.65	1.13	0.17	0.51	0.36	0.02	0.07	0.07	0.51	0.56	2.34	1.85
Al_2O_3	30.63	21.62	27.45	25.32	20.59	22.74	20.59	19.05	17.05	30.01	17.14	19.04	34.00	29.69	21.82	36.49	32.61	19.85	21.09
Fe_2O_3																			
FeO	2.89	6.82	3.10	4.24	5.74	5.39	7.56	5.75	8.4	2.00	5.00	5.34	3.82	2.66	25.10	1.01	2.56	11.16	14.63
MnO	0.02	0.07	0.05	0.03	0.04	0.03	0.08	0.04	0.15	0.03	0.04	0.05	0.01	0.00	0.25	0.01	0.02	0.13	0.14
MgO	1.62	3.31	2.07	2.43	2.49	2.56	3.73	2.77	4.05	1.14	2.16	2.54	0.67	0.98	13.69	0.75	1.03	6.83	5.46
CaO	0.40	0.58	0.42	0.41	0.64	0.50	1.17	0.72	1.12	1.05	1.78	2.26	0.10	0.16	0.04	0.03	0.53	0.35	0.89
Na_2O	0.43	1.21	0.71	1.04	0.90	1.37	1.02	0.90	0.64	0.25	0.99	0.85	0.49	0.09	1.70	0.82	0.89	0.47	0.00
K_2O	2.82	4.88	6.59	5.62	3.33	4.43	3.83	3.25	3.22	2.28	3.18	2.30	0.15	2.15	0.12	8.09	8.60	5.64	6.31
Total	87.05	87.23	87.03	79.34	79.34	82.92	77.93	74.41	74.08	82.23	70.01	73.86	81.51	81.57	87.97	95.85	95.12	95.35	95.97
Si	3.332	3.427	3.321	3.383	3.485	3.405	3.213	3.432	3.265	3.301	3.481	3.435	2.834	3.043	2.798	3.084	3.210	3.324	3.178
^{IV}Al	0.668	0.573	0.679	0.617	0.515	0.595	0.787	0.568	0.735	0.699	0.519	0.565	1.166	0.957	1.202	0.916	0.790	0.676	0.822
TC	0.668	0.573	0.679	0.617	0.515	0.595	0.787	0.568	0.735	0.699	0.519	0.565	1.166	0.957	1.202	0.916	0.790	0.676	0.822
Ti	0.015	0.041	0.011	0.024	0.037	0.020	0.014	0.040	0.073	0.010	0.034	0.023	0.001	0.004	0.005	0.025	0.028	0.122	0.098
^{VI}Al	1.805	1.254	1.625	1.509	1.366	1.409	1.176	1.299	0.978	1.878	1.274	1.309	1.511	1.391	1.483	1.889	1.759	0.938	0.928
Fe(III)	0.166	0.409	0.184	0.253	0.372	0.337	0.511	0.400	0.599	0.122	0.371	0.373							
Fe(II)													0.214	0.149	2.191	0.055	0.142	0.644	0.861
Mn	0.001	0.005	0.003	0.002	0.003	0.002	0.005	0.003	0.011	0.002	0.003	0.004	0.000	0.000	0.022	0.001	0.001	0.007	0.008
Mg	0.165	0.353	0.219	0.258	0.288	0.285	0.436	0.343	0.477	0.124	0.286	0.316	0.066	0.098	2.131	0.060	0.102	0.698	0.543
TOC	1.999	2.062	2.042	2.046	2.066	2.053	2.142	2.085	2.138	2.136	1.968	2.025	1.792	1.642	5.832	2.030	2.032	2.409	2.438
OC		0.131	0.085	0.098	0.056	0.108	0.001	0.051	0.001		0.351	0.222		1.317		0.001	0.121	0.000	0.000
Mg							0.014		0.038							0.013		0.005	0.030
Ca	0.029	0.045	0.032	0.032	0.053	0.040	0.102	0.064	0.102	0.082	0.169	0.202	0.007	0.011	0.004	0.002	0.038	0.026	0.067
Na	0.057	0.168	0.098	0.144	0.135	0.199	0.159	0.145	0.106	0.035	0.170	0.137	0.044	0.064	0.019	0.214	0.105	0.119	0.064
K	0.247	0.446	0.599	0.511	0.329	0.423	0.395	0.345	0.350	0.212	0.360	0.245	0.013	0.184	0.016	0.673	0.728	0.496	0.567
ILC		0.704	0.761	0.719	0.570	0.702	0.786	0.618	0.736		0.868	0.786		0.270		0.917	0.909	0.677	0.825
TLC		0.704	0.764	0.715	0.571	0.703	0.788	0.619	0.736		0.870	0.787		2.274		0.917	0.911	0.676	0.822
OH-	2	2	2	2	2	2	2	2	2	2	2	2	8	8	8	2	2	2	2
Total	6.486	6.721	6.772	6.731	6.583	6.715	6.813	6.639	6.734	6.463	6.667	6.61	5.856	5.901	9.871	6.932	6.903	7.055	7.165

Chlorite is calculated on the basis of 14 oxygens/8(OH) and all Fe as FeO. Kaolinite is calculated on the basis of 7 oxygens/4(OH). Mica and illite are calculated on basis of 11 oxygens/2(OH) and all Fe as FeO and Fe_2O_3, respectively. Illite-smectite is calculated on the basis of 11 oxygens/2(OH), all Fe as Fe_2O_3, and no interlayer water. TC = tetrahedral charge, TOC = total octahedral cation, OC = octahedral charge, ILC = interlayer charge, TLC = total layer charge, Fe(II) = divalent Fe.

Kaolinite and mixed-layer kaolinite-smectite. The diffraction peaks at ~7.22 (d_{001}) and 3.63 Å (d_{002}) were diagnostic of the presence of kaolinite in sediments analyzed. Although relatively well defined and symmetrical, the kaolinite second basal diffraction peak showed a tail in the low-angle region (Figures 3–4), suggesting the presence of minor interstratified 2:1 clay minerals, presumably smectite (*e.g.* Dudek *et al.*, 2006; Hong *et al.*, 2012). The EG solvation showed an increase in the d_{001} peak of kaolinite, while the low-angle shoulder migrated toward higher *d* values. The shift in the tail that takes place after glycolation, from ~7.4 to 7.8 Å, is normally considered as evidence of smectite interlayering (Schultz *et al.*, 1971). Hence, apart from the kaolinite d_{001} diffraction peak to fit XRD spectra (Figure 4), a disordered R0 K-S with a maximum at ~7.4 Å and up to 7 wt.% of the smectite component (Table 1) was used. Kaolinite particles are well dispersed within the illite-dominated matrix, forming aggregates with sizes from 10 to 20 μm devoid of characteristic shapes (Figure 6b).

Mineral-phase chemistry

The representative mineral chemistry of selected clay minerals from the SNS sediment are reported along with few analyses of coarser mica and kaolinite that served as a reference (Table 4). The composition of chlorite is characterized by a total cation content of slightly <10, suggesting a dominance of divalent Fe, resulting in the classification of the chlorites as trioctahedral. Accordingly, the chlorite may be defined as pycnochlorite (X_{Fe} = 51) (Hey, 1954). The kaolinite composition is non-stoichiometric given the Si depletion (2.83–3.04 a.p.f.u.) and Fe enrichment (0.15–0.21 a.p.f.u.). This may be attributed to the development of porosity between packets of kaolinite, the presence of micron-scale impurities in the form of Fe-Ti bearing minerals, or smectite interlayering (*e.g.* Cuadros and Altaner, 1998; Sengupta *et al.*, 2008). Regardless of the variable valence of Fe, the total octahedral cation content of mica was <2.5 a.p.f.u. (2.03–2.04 and 2.41–2.47 for muscovite and biotite, respectively), which, according to Rieder *et al.* (1998), defined them as dioctahedral mica. The biotite composition covers the compositions between $1.614 \leqslant ({}^{IV}Al + {}^{VI}Al) \leqslant 1.750$ a.p.f.u., while for muscovite the ($^{IV}Al + {}^{VI}Al$) ranged between 2.549 and 2.805 a.p.f.u. (^{IV}Al and ^{VI}Al stand for tetrahedral and octahedral Al, respectively). Both micas are characterized by variable levels of Mg, Fe, and Ti substituting for octahedral Al (phengite substitution). K-rich white mica referred to here as 'muscovite' is of phengitic composition ($Si \geqslant 3.1$ a.p.f.u., Rieder *et al.*, 1998). The average phase chemistry of illites (illite *sensu stricto*, R3 I-S) and mixed-layer illite-smectite (R0 I-S, R0 I-SS) is $(Ca_{0.034}K_{0.451}Na_{0.117})(Al_{1.548}Fe(III)_{0.253}Mg_{0.249}Ti_{0.023})^{VI}(Si_{3.366}Al_{0.634})^{IV}O_{10}[(OH)_2,(H_2O)]$ (16 analyses) and $(Ca_{0.102}K_{0.332}Na_{0.136})(Al_{1.336}Fe(III)_{0.386}Mg_{0.326}Ti_{0.031})^{VI}(Si_{3.377}Al_{0.623})^{IV}O_{10}(OH)_2{\cdot}nH_2O$ (45 analyses), respectively. In the EMPA data presentation, all the mixed-layer I-S species used for XRD profile fitting were referred to arbitrarily as mixed-layer I-S. As reported by Norrish and Pickering (1983), the K_2O content in illite-like phases is inversely related to that of H_2O (Table 4). When comparing illite and interstratified I-S, the latter is characterized by an elevated Ca content, up to 0.169 Ca p.f.u. In the case of K, an inverse trend was reported, with I-S rich in Ca being depleted in K content (Figure 8a). A similar distinction was inferred from the occupancy of tetrahedral and octahedral sites (Figure 8b), with illite showing a larger amount of ^{IV}Al (hence less Si, Table 4), whereas mixed-layer minerals were characterized by elevated abundances of octahedral Fe and Mg. For those I-S with the largest proportions of octahedral Fe and Mg (samples 310 and 350, Table 4), some of the Mg was allocated into the interlayer structural position in order to respect the maximal cation occupancy per octahedral sheet. Such peculiar phase chemistry can be explained by restricted chlorite interlayering (~10%), which gives rise to the formation of mixed-layer illite-chlorite-smectite clays (Weaver and Beck, 1971). Somewhat larger water contents documented in I-S from samples 310 and 350 (Table 4) conform to this line of reasoning. Regarding the compositions of pure smectites and nearly pure smectites (I-S with >80 wt.% smectite: Boles and Franks (1979), Ramseyer and Boles (1986) and references therein) and that of illites with <10 wt.% of the smectite component (Deer *et al.*, 1996; Meunier and Velde, 2004), the illites and I-S analyzed in the present study are projected in the lower segment of the illite compositional field, while some of the I-S analyses approached the composition of smectite-rich I(0.2)–S(0.8) (Figure 8b). The mixed-layer smectite component is defined as dioctahedral and close to beidellite in composition (Table 4; Grim, 1968).

Clay-mineral distribution

The clay-mineral investigation of sediments from borehole K14-12 in the Dutch North Sea showed illite and kaolinite as well as their smectite interstratifications as dominant clay phases (illite *sensu stricto* + R3 I-S 34–52 wt.%; illite-smectite (R0 I-S, R0 I-SS) 22–41 wt.%; kaolinite 7–10 wt.%; kaolinite-smectite 7–20 wt.%; Table 3). The largest amounts of illite (illite and R3 I-S) were recorded in the overlying unit (sample 220) with slightly smaller amounts in Unit B (sample 240) and in the pre-glacial deposits (sample 530; Figure 7). These values coincided with the smallest amounts of I-S and, consequently, with the smallest proportions of the total smectite component (Sme_{TOT}: total smectite content from all I-S present, Table 3). Unit A, representing the clinoform TV infill (samples 310, 350, 370, and 440), was characterized by smaller illite abundances coupled with elevated I-S and Sme_{TOT}.

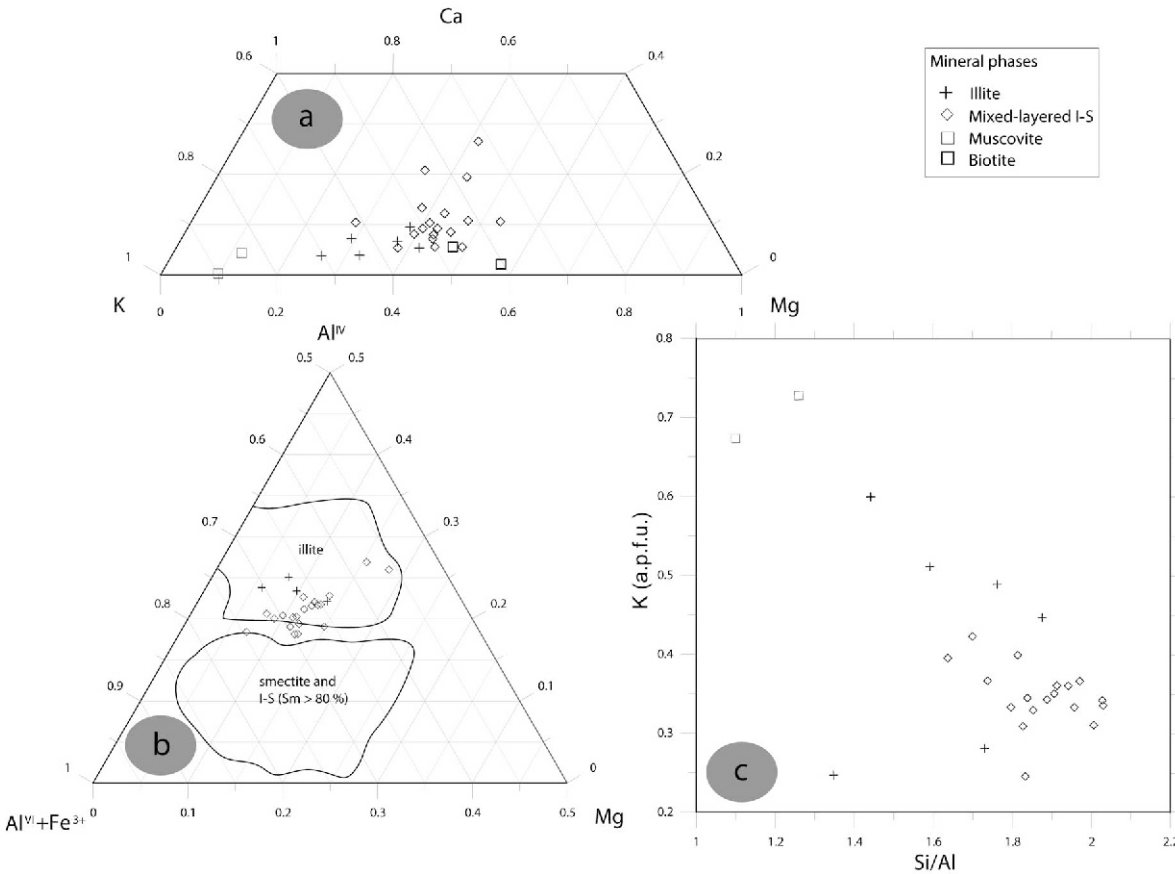

Figure 8. Mineral differentiation diagrams based on the phase chemistry of micas, illite, and interstratified I-S. (a) Ca-K-Mg ternary diagram showing a trend of Ca and Mg enrichment in the illite and I-S; (b) $^{IV}Al-{}^{VI}Al+Fe(III)-Mg$ ternary diagram (superscripts IV and VI refer to tetrahedral and octahedral sheets, respectively) illustrating the changes in octahedral composition reflecting a smectitization process; and (c) K–Si/Al plot depicting the relationship of interlayer K net loss with Al-Si replacement during smectitization. For details, see the text.

The latter is, thus, inferred to have maximal concentrations in the central portions of the TV infill (samples 350 and 370 with 20 and 18 wt.% Sme_{TOT}, respectively, Table 3; Figure 2c). In contrast, the kaolinite (kaolinite + R0 K-S) content is greatest in pre-glacial sediments, whereas in the TV succession it maintained a uniform proportion at ~20 wt.%, except in the uppermost unit where it was even smaller (Table 3).

DISCUSSION

The area of the SNS offers an opportunity to investigate the provenance and 'source-to-sink' transport of terrigenous material in a marginal sea (*e.g.* Irion and Zöllmer, 1999; Leipe and Sea, 2003; Kuhlmann *et al.*, 2004; Nielsen *et al.*, 2015; Griffioen *et al.*, 2016). Clay minerals, in particular, may serve as effective tools to establish the origin of fine-grained terrigenous sediment. In the area studied, clay minerals consist mainly of illite and mixed-layer illite-smectite with minor kaolinite and chlorite (Table 3). In depositional eogenetic environments, illite as well as kaolinite and chlorite do not form; therefore, when found in sediments that have not suffered deep-burial diagenesis, they are considered as detrital rather than neoformed (Meunier and Velde, 2004). Illite KI values (0.415–0.341°Δ2θ), although somewhat compromised by smectite interlayering (R3 I-S with d_{001} 10.08–10.14 Å; Figure 5), provide additional evidence of the detrital nature of the illite (*e.g.* Ferreiro Mählmann *et al.*, 2012). The size of illite particles (~ 5–10 μm, Figure 7a) and its flaky particle structure (Figure 6a) are also features that suggest the detrital origin of the illite (Iacoviello *et al.*, 2012).

The succession analyzed consists of different units characterized by similar mineralogy of the clay fraction. The most striking feature in terms of clay composition is the lack of discrete smectite, which suggests little input from central European rivers before and after the Elsterian glaciation (Kuhlmann *et al.*, 2004; Adriaens, 2015; Griffioen *et al.*, 2016). Knowing that during the upper Early Pleistocene, the material transport by the BRS had practically stopped, the sediment of the TV

https://doi.org/10.1346/000986016820500438 Published online by Cambridge University Press

infill can be considered as glaciogenic, older smectite-free material that was eroded locally during the formation of TV. In the TV sequence analyzed no discrete smectite was observed and illite along with illite-rich I-S are the dominant clay species (Table 3). Within the TV sediment section studied the distribution of smectite-rich I-S (R0 I-S + R0 I-SS, Table 1) was shown to be of particular importance. Namely, I-S displayed maximal abundances in the TV infill (Unit A, Figure 2c), while it appears in significantly smaller amounts in Units B and C and in the pre-glacial deposits (Table 3). The same pattern is inferred for the total smectite content (Sme_{TOT}) calculated from all I-S species identified (Tables 1, 3). Within Unit A, those horizons are reported that have been exposed to the influence of meltwater for the longest period of time (earliest clinoforms), *i.e.* which have the largest Sme_{TOT} values (samples 350–440; Figure 2; Table 3). Such indicative distributions of I-S in sediments of analyzed Elsterian TV, along with the known impoverishment of reworked pre-glacial sediments in smectite and I-S, suggest the *in situ* alteration of illite to illite-smectite (smectitization) as the most plausible explanation of smectite interlayering in the clays analyzed. The process of mineral transformation of stable clay phases (*i.e.* illite) to open minerals featured by variable basal spacings (*i.e.* I-S) assumes a loss of substance, which is, therefore, occasionally referred to as degradation (Millot, 1971). Usually, such a mineral transformation takes place in soils and weathering crust affected by degrading fluids (Whittig and Jackson, 1955; Jackson, 1957; Fordham, 1990). In sedimentary environments, however, the alteration of illite is rarely documented (Smoot, 1960), which is explained readily by restrained matter exchange (Hartmann *et al.*, 1999). Smectitization in analyzed sediments must have occurred by inhibited early chemical diagenesis in a freshwater environment of fluvial or lacustrine nature where meltwater played the role of degrading fluid that percolated through the eroded TV pre-glacial sediment of SNS at glacial maximum when seawater conditions faded away (de Gans, 2007). Such a diagenetic process itself is not isochemical because it requires mobilization of a wide range of elements such as K, Ca, Fe, and Mg, as well as Al and Si. After the sediment re-deposition within TV, the detrital illite that survived initial weathering and physical erosion reacted with freshwater, giving rise to a range of I-S species (Chamley, 1989 and references therein; Figure 5; Table 3). The smectitization of illite is hypothesized here to have operated in this study area by reaction with cold freshwater by means of a series of mixed-layer intermediates (I-S) with illite being converted to low-charged smectite layers. Most of the total charge remained within the tetrahedral sheet, even in I-S with the greatest smectite abundances (Table 4). The first expression of the smectitization process was the emergence of ordered R3 I-S with up to 13 wt.% of the smectite component (Table 1; Figure 5) as a consequence of an initial decrease of K content from ~0.45 to ~0.35 a.p.f.u. This makes a net loss of ~0.10 a.p.f.u. compared to an average illite composition (Table 4; Figure 8c). At the same time, Si replaced Al in the tetrahedral sheet at an initial compositional difference of ~0.005–0.01 a.p.f.u. (Table 4; Figure 8c). Geochemical data do not show released Al to be accommodated in the octahedral sheet of a newly formed smectite component; neither was it found building hydroxy interlayers (gibbsite sheet) that would eventually lead to the appearance of hydroxy-interlayered smectite (HIS; Meunier, 2007; Table 4; Figure 3). Aluminum was instead leached from the structure of the newly formed mixed-layer I-S, and some of it may have been consumed by neoformation of minute crystallites of kaolinite found in the sediment matrix. The charge imbalance in I-S caused by the K loss and tetrahedral rearrangements is accommodated by Mg and Fe(III) liberated from altered chlorite and biotite (average increase of 0.1 and 0.2 a.p.f.u., respectively; Table 4; Figure 8b). In I-S where the greatest concentrations of Mg and Fe (>0.9 a.p.f.u.) are reported (Table 4), some of the Mg is accommodated in the interlayer site, suggesting a restrained chlorite interlayering in smectite-rich illite-smectite (~10%; Weaver and Beck, 1971). Finally, Ca enters the structure, partly filling the interlayer site, such that the I-S is enriched in Ca by ~0.02 a.p.f.u. with respect to illite (Table 4; Figure 8a). The retention of Si and Ca in the products of smectitization indicates that these usually easily leached elements (Schaetzl and Thompson, 2015) were retained in the diagenetic environment. Smaller particles (0.04–0.08 μm; Figure 7a), having comparatively larger reaction surfaces, are probably disordered R0 I-S and R0 I-SS (Table 1; Figure 5), showing advanced smectitization in the form of maximal loss of K (~0.25 a.p.f.u.; Table 4; Figure 8c) and minimal tetrahedral Al values (~0.55 a.p.f.u.; Table 4). The composition of the octahedral sheet, having maximal Fe(III) abundances (~0.55 a.p.f.u.; Table 4) approaches I-S compositions with ~80 wt.% smectite (Figure 8b; Boles and Franks, 1979; Ramseyer and Boles, 1986), which is consistent with the composition of R0 I-SS defined by XRD modeling to have ~75–94 wt.% smectite layers (Table 1). An incomplete evolution of illite toward smectite composition may thus be inferred to be an evolutionary sequence represented by I-S phases of different ordering degree, smectite content, and mineral chemistry.

The smectitization reaction progress is controlled mainly by the particle size of detrital illite, with additional influence by other common factors such as climate, sediment porosity and permeability, and fluid composition (Schaetzl and Thompson, 2015). Based on XRD mineral composition (Table 3) and grain-size data, the two principal components that cover ~75% of the

total variance in a PCA space define a coherent group of samples belonging to Unit A and, thus, to the peak smectitization, while the samples of pre-glacial and overlying sediments are clearly outliers (Figure 7b; Table 1). The role of the grain size becomes even more apparent in the variable projection plot (Figure 7a) in which the grain-size classes are shown as supplementary variables with the finest fraction corresponding to smectite-rich disordered I-S and the coarsest to detrital illite and chlorite. Such a relationship points clearly to larger reaction surfaces of small illite particles that promote smectitization by allowing more fluid–rock interaction, leading to enhanced chemical exchange between solid and fluid phases.

Proposed here is that the formation of mixed-layer I-S described above took place in a freshwater, ice-marginal to proglacial, depositional environment during the glacial maximum. The progressive ice-sheet withdrawal coeval to sediment accumulation at the ice-margin caused a northward shift of the depositional environment. Accordingly, the remaining ice-marginal sediments were exposed to the restrained influx of freshwater, in the form of meltwater, as the ice-sheet retreated giving rise to a reduced elemental leaching and mineral transformations (Hartmann *et al.*, 1999). This contribution thus confirms that the marine depositional environment was absent during the glacial episode in the SNS (de Gans, 2007). Nowadays, a generally accepted view is that the composition of ocean-floor clays primarily reflects the continental sediment supply (*e.g.* Biscaye, 1965; Griffin *et al.*, 1968; Petschick *et al.*, 1996). Once settled in seawater, the continental clay minerals are apparently inert but their exchange capacity is no longer saturated by the same cations (Sayles and Mangelsdorf, 1977). Moreover, the seawater-rich cations such as K, Na, and Mg have been shown to be preferentially depleted in waters impregnating the onset of ocean floors (Sayles, 1981), thus presumably giving rise to the neoformation of ordered clay minerals such as illite and chlorite by fixation of ions from seawater (*e.g.* Grim and Johns, 1954). This mechanism is seemingly contrary to the early diagenetic smectitization proposed here.

The continuity of the freshwater environment beyond the ice-margin in a proglacial lake that covered the whole clinoform succession is furthermore suggested by seismic reflection data (Benvenuti and Moscariello, 2016). Although very little sedimentological and mineralogical evidence for a proglacial lake in the central part of the SNS is provided in the literature, this contribution supports the studies of Gibbard (2007) and Gupta *et al.* (2007) who were first to hypothesize the existence of a large proglacial lake at the glacial maximum in the area between the SNS and the Benelux countries. The lacustrine episode in the study area ended with the Holstenian transgression and marine sedimentation that covered the lacustrine deposits on a regional scale, as reported from several occurrences of onshore TVs in the northern part of Germany and The Netherlands (Ehlers and Gibbard, 2004).

The hydromorphic conditions of the glacial period that left traces in clay mineralogy of Unit A (*i.e.* I-S formation, Figure 1) suggest an excess of silica released from dissolved feldspar and quartz (Table 2) that were required for enhanced smectitization (*e.g.* Novikoff *et al.*, 1972). In contrast, in the areas where hydromorphic influences were weaker, or acted for a more restricted time, lesser amounts of interlayered phases were produced, as shown by lesser abundances of I-S in the uppermost part of Units A, B, and C. The low I-S content of Unit C may, however, be attributed to the return of marine conditions, in line with the more widespread distribution of the deposits of Unit C around the TV boundaries, which coincides with the progressive end of the glacial lacustrine environment at the onset of the Holstenian interglacial (Ehlers and Gibbard, 2004). The presence of I-S in marine pre-glacial deposits, even if in lower percentages than in the TV infill, may still be related to early diagenetic smectitization operating during the glacial stage and facilitated by the large amount of meltwater that percolated into the underlying deposits for hundreds of meters (Kehew *et al.*, 2012 and references therein).

The presence of I-S in sedimentary rocks is traditionally interpreted through the prism of deep-burial diagenesis. Mixed-layer I-S reported from shallower levels of sedimentary sequences (<1 km) is rarely described in diagenetic studies, mostly due to lack of economic interest. This study offered an alternative approach to the evolution of clay assemblages by studying geologically unique glacial environments such as TVs, where the I-S interstratification is linked to early (shallow) diagenesis (smectitization) of detrital illite (and lesser kaolinite). The multi-methodological approach used in the present study could be applied to clay research of sediment accumulations that are related to Pleistocene glacial events and currently reported extensively in the area of the North Sea, in order to better understand the early diagenesis portion of the clay cycle examined in the present research.

CONCLUSIONS

(1) Material analyzed from borehole K14-12 located in the K block of Dutch offshore presented a thick succession of Elsterian TV deposits consisting of several units (pre-glacial, A, B, and C) visible on seismic sections.

(2) Grain-size distributions are relatively heterogeneous, with the lower part of succession (lower Unit A) dominated by coarse sand. Higher in the succession, the grain size becomes finer with up to 20 wt.% of clay content in the upper portions of Unit A (TV infill), as well as in Units B and C.

https://doi.org/10.1346/000986016820500438 Published online by Cambridge University Press

(3) Bulk-rock mineralogy of the material analyzed is dominated either by quartz or illite, depending on the sediment granulometry. Other phases, notably feldspar and mica, constitute <10 wt.%.

(4) Measurements by XRD and SEM showed a clay-particle assemblage consisting of illite, mixed-layer illite-smectite, kaolinite, and chlorite, with the first and the second being the dominant clay minerals.

(5) Illite is inferred, according to its mineralogical and morphological characteristics (Kübler index, particle size, and shape), to have an unambiguously detrital origin.

(6) The abundances of clay minerals in the stratigraphic succession studied show interlayered I-S enriched in the middle portion of Unit A where illite abundance is less. I-S abundance was less in the pre-glacial unit and, especially, in the overlying Units B and C. X-ray diffraction pattern modeling and deconvolution revealed interlayered I-S to consist of several intermediate phases of different ordering and composition grouped as non-swelling ordered I-S (illite *sensu stricto* + R3 I-S) and disordered I-S (R0 I-S + R0 I-SS).

(7) The hypothesis of smectitization of illite in a freshwater diagenetic environment is supported by the distribution patterns of I-S, the total smectite (Sme_{TOT}), and I-S particle sizes. The smectitization of illite proceeded in a way in which extensive leaching was precluded.

(8) The I-S phase chemistry and speciation of I-S interlayers revealed by modeling of XRD spectra shows that smectitization must have proceeded through a series of mixed-layer I-S intermediates, whereby the illite component was converted progressively to smectite. The chemistry of the I-S octahedral sheet suggests that interlayers with maximal Fe content approach I-S compositions with 80 wt.% of smectite component, thus corresponding to R0 I-SS as defined by XRD pattern modeling (75–94 wt.% smectite). Moreover, the structural formulae of smectite-rich I-S point to the partial allocation of Mg in their interlayer site, which is indicative of restrained chlorite interlayering (~10%) and possible formation of illite-chlorite-smectite clays.

(9) In addition to factors such as climate, porosity and permeability, and fluid composition, the grain size of illite particles influences the progress of smectitization as shown by PCA analysis through a variable load plot where, in addition to the XRD mineralogy, the grain-size classes are shown as supplementary variables.

(10) The results of the present study are consistent with the hypothesis that formation of mixed-layer I-S by incomplete diagenetic alteration of detrital illite took place in an ice-marginal to proglacial freshwater depositional environment where meltwater must have played the role of degrading fluid responsible for enhanced ion exchange.

ACKNOWLEDGMENTS

The present study was supported financially by the GRASP consortium. The Nederlandse Aardolie Maatschappij (Shell) is thanked for providing the sediment material from borehole K14-12. The authors thank P. Gibbard for use of his data on the extent of the Pleistocene ice-sheets. F. Gischig is thanked for the outstanding quality of the thin and polished sections produced for QEMSCAN®, SEM-EDS, and EMPA investigations. R. Cerny is acknowledged for providing excellent working conditions during extensive XRD measurements. Appreciation is addressed to S. Carmalt and A. Ristić for their assistance with the English. The authors also thank L. Dominguez and S. Biass and the whole Physical Volcanology and Geological Risk research group in Geneva for use of the grain-size analyzer and for their help in using the instrument. Critical comments by A. Süssenberger helped to improve an early version of the manuscript and the support of A. Janszen regarding the material provided is also appreciated. The manuscript improved significantly due to the review of H. Yalçin. Special thanks to P. Schroeder for his editorial handling.

REFERENCES

Adriaens, R. (2015) Neogene and Quaternary clay minerals in the Southern North Sea. PhD thesis, University of Leuven, Belgium, 272 pp.

Aitchinson, J. (1982) The statistical analysis of compositional data. *Journal of the Royal Statistical Society, Series B*, **44**, 139–177.

Allmann, R. (2003) *Röntgen-Pulverdiffraktometrie*. Springer Berlin, Heidelberg, 275 pp.

Benvenuti, A. and Moscariello, A. (2016) High-resolution seismic geomorphology and stratigraphy of a tunnel valley confined ice-margin fans (Elsterian glaciation, southern North Sea). *Interpretation*, **4**, T461–T483.

Bijlsma, S. (1981) Fluvial sedimentation from the Fennoscandian area into the north-west European basin during the Late Cenozoic. *Geologie en Mijnbouw/ Netherlands Journal of Geosciences*, 337–345.

Biscaye, P.E. (1965) Mineralogy and sedimentation of recent deep-sea clay in the Atlantic Ocean and adjacent seas and oceans. *Geological Society of America Bulletin*, **76**, 803–832.

Blott, S.J. and Pye, K. (2001) GRADISTAT: a grain size distribution and statistics package for the analysis of unconsolidated sediments. *Earth Surface Processes and Landforms*, **26**, 1237–1248.

Boles, J.R. and Franks, S.G. (1979) Clay diagenesis in Wilcox sandstones of Southwest Texas: Implications of smectite diagenesis on sandstone cementation. *Journal of Sedimentary Research*, **49**, 55–70.

Brown, G. and Brindley, G.W. (1980) X-ray diffraction procedures for clay mineral identification. Pp. 305–306 in: *Crystal Structures of Clay Minerals and their X-Ray Identification*. Monograph **5**, Mineralogical Society, London.

Chamley, P.D.H. (1989) *Terrigenous Supply in the Ocean*. Springer, Berlin Heidelberg, pp. 163–192.

Cohen, K.M. and Gibbard, P.L. (2010) Global chronostratigraphical correlation table for the last 2.7 million years, v. 2010. *Journal of Quaternary Science*, **2**, 7.

Cuadros, J. and Altaner, S.P. (1998) Characterization of mixed-layer illite-smectite from bentonites using microscopic, chemical, and X-ray methods: Constraints on the smectite-to-illite transformation mechanism. *American Mineralogist*, **83**, 762–774.

de Gans, W. (2007) Quaternary. Pp. 173–195 in: *Geology of the Netherlands* (T.E. Wong, D.A.J. Batjes, and J. de Jager, editors). Royal Netherlands Academy of Arts and Sciences.

Deer, W.A., Howie, R.A., and Zussman, J. (1996) *An Introduction to the Rock-Forming Minerals*. 2nd edition. Prentice Hall, Harlow, Essex, England, New York, 712 pp.

Drits, V.A. and Sakharov, B.A. (1976) *X-ray Structural Analysis of Mixed-Layer Minerals*. Nauka, Moscow.

Drits, V. A. (2003) Structural and chemical heterogeneity of layer silicates and clay minerals. *Clay Minerals*, **38**, 403–432.

Dudek, T., Cuadros, J., and Fiore, S. (2006) Interstratified kaolinite-smectite: Nature of the layers and mechanism of smectite kaolinization. *American Mineralogist*, **91**, 159–170.

Eberl, D.D. and Velde, B. (1989) Beyond the Kübler index. *Clay Minerals*, **24**, 571–577.

Ehlers, J. and Gibbard, P.L. (editors) (2004) *Quaternary Glaciations Extent and Chronology Part I: Europe*. 475 pp.

Ferrage, E., Lanson, B., Sakharov, B.A., and Drits, V.A. (2005) Investigation of smectite hydration properties by modeling of X-ray diffraction profiles. Part 1. Montmorillonite hydration properties. *American Mineralogist*, **90**, 1358–1374.

Ferreiro Mählmann, R., Bozkaya, Ö., Potel, S., Bayon, R.L., Šegvić, B., and Nieto, F. (2012) The pioneer work of Bernard Kübler and Martin Frey in very low-grade metamorphic terranes: Paleo-geothermal potential of variation in Kübler-Index/organic matter reflectance correlations. A review. *Swiss Journal of Geosciences*, **105**, 121–152.

Folk, R.L. and Ward, W.C. (1957) Brazos River bar [Texas]: A study in the significance of grain size parameters. *Journal of Sedimentary Petrology*, **27**, 3–26.

Fordham, A.W. (1990) Weathering of biotite into dioctahedral clay minerals. *Clay Minerals*, **25**, 51–63.

Gibbard, P.L. (2007) Europe cut adrift. *Nature*, **448**, 259,260.

Gottlieb, P., Wilkie, G., Sutherland, D., Ho-Tun, E., Suthers, S., Perera, K., Jenkins, B., Spencer, S., Butcher, A., and Rayner, J. (2000) Using quantitative electron microscopy for process mineralogy applications. *The Journal of The Minerals, Metals & Materials Society (TMS)*, **52**, 24–25.

Griffin, J.J., Windom, H., and Goldberg, E.D. (1968) The distribution of clay minerals in the world ocean. *Deep-Sea Research*, **15**, 433–459.

Griffioen, J., Klaver, G., and Westerhoff, W.E. (2016) The mineralogy of suspended matter, aquatic and Cenozoic sediments in the Rhine-Meuse-Scheldt delta area, the Netherlands: An overview and review. *Netherlands Journal of Geosciences*, 1–85.

Grim, R.E. (1968) *Clay Mineralogy*. 2nd edition. McGraw-Hill Book Company, Inc., New York, 596 pp.

Grim, R.E. and Johns, W.D. (1954) Clay mineral investigation of sediments in the Northern Gulf of Mexico. *Clays and Clay Minerals*, **2**, 81–103.

Guggenheim, S., Bain, D.C., Bergaya, F., Brigatti, M.F., Drits, A., Eberl, D.D., Formoso, M.L.L., Galan, E., Merriman, R.J., Peacor, D.R., Stanjek, H., and Watanabe, T. (2002) Report of the AIPEA nomenclature committee for 2001: order, disorder and crystallinity in phyllosilicates and the use of the 'Crystallinity Index'. *Clay Minerals*, **37**, 389–393.

Gupta, S., Collier, J.S., Palmer-Felgate, A., and Potter, G. (2007) Catastrophic flooding origin of shelf valley systems in the English Channel. *Nature*, **448**, 342–345.

Harding, R. (2015) Evolution of the giant southern North Sea shelf prism: Testing sequence stratigraphic concepts and the global sea level curve with full three dimensional control. PhD thesis, University of Manchester, UK.

Hartmann, B.H., Juhász Bodnár, K., Ramseyer, K., and Matter, A. (1999) Effect of Permo-Carboniferous climate on illite-smectite, Haushi Group, Sultanate of Oman. *Clays and Clay Minerals*, **47**, 131–143.

Hey, M. (1954) A new review of the chlorites. *Mineralogical Magazine*, **30**, 277–292.

Hong, H., Churchman, G.J., Gu, Y., Yin, K., and Wang, C. (2012) Kaolinite–smectite mixed-layer clays in the Jiujiang red soils and their climate significance. *Geoderma*, **173-174**, 75–83.

Huggett, J.M. and Knox, R.W.O. (2006) Clay mineralogy of the Tertiary onshore and offshore strata of the British Isles. *Clay Minerals*, **41**, 5–46.

Huuse, M. and Lykke-Andersen, H. (2000) Overdeepened Quaternary valleys in the eastern Danish North Sea: Morphology and origin. *Quaternary Science Reviews*, **19**, 1233–1253.

Iacoviello, F., Giorgetti, G., Nieto, F., and Memmi, I. (2012) Evolution with depth from detrital to authigenic smectites in sediments from AND-2A drill core (McMurdo Sound, Antarctica). *Clay Minerals*, **47**, 481–498.

Irion, G. and Zöllmer, V. (1999) Clay mineral associations in fine-grained surface sediments of the North Sea. *Journal of Sea Research*, **41**, 119–128.

Jackson, M.L. (1957) Frequency distribution of clay minerals in major great soil groups as related to the factors of soil formation. *Clays and Clay Minerals*, **6**, 133–143.

Kehew, A.E., Piotrowski, J.A., and Jørgensen, F. (2012) Tunnel valleys: Concepts and controversies – A review. *Earth-Science Reviews*, **113**, 33–58. Elsevier B.V., Amsterdam.

Kemp, S.J. and Merriman, R.J. (2009) Polyphase low-grade metamorphism of the Ingleton Group, northern England, UK: A case study of metamorphic inversion in a mudrock succession. *Geological Magazine*, **146**, 237–251.

Kretz, R. (1983) Symbols for rock-forming minerals. *American Mineralogist*, **68**, 277–279.

Kübler, B. (1964) Les argiles, indicateurs de métamorphisme. *Revue de l'Institut Français du Pétrole*, **19**, 1093–1112.

Kuhlmann, G., de Boer, P.L., Pedersen, R.B., and Wong, T.E. (2004) Provenance of Pliocene sediments and paleoenvironmental changes in the southern North Sea region using Samarium–Neodymium (Sm/Nd) provenance ages and clay mineralogy. *Sedimentary Geology*, **171**, 205–226.

Laban, C. (1995) The Pleistocene glaciations in the Dutch sector of the North Sea. PhD thesis, University of Amsterdam, The Netherlands.

Lagaly, G., Ogawa, M., and Dékány, I. (2006) Clay mineral organic interactions. Pp. 309–377 in: *Handbook of Clay Science* (F. Bergaya, B.K.G. Theng, and G. Lagaly, editors). Developments in Clay Science, Elsevier, Amsterdam.

Lanson, B. (1993) *DECOMPXR, X-ray diffraction pattern decomposition program*. ERM, Poitiers, France, 48 pp.

Lanson, B. and Besson, G. (1992) Characterization of the end of smectite-to-llite transformation: Decomposition of X-ray patterns. *Clays and Clay Minerals*, **40**, 40–52.

Lanson, B. and Velde, B. (1992) Decomposition of X-ray diffraction patterns: A convenient way to describe complex I-S diagenetic evolution. *Clays and Clay Minerals*, **40**, 629–643.

Lê, S., Josse, J., and Husson, F. (2008) FactoMineR: An R package for multivariate analysis. *Journal of Statistical Software*, **25**, 1–18.

Lee, J.R., Busschers, F.S., and Sejrup, H.P. (2012) Pre-Weichselian Quaternary glaciations of the British Isles, The Netherlands, Norway and adjacent marine areas south of 68N. implications for long-term ice sheet. *Quaternary Science Reviews*, **44**, 213–228.

Leipe, T. and Sea, B. (2003) The kaolinite/chlorite clay mineral ratio in surface sediments of the southern Baltic Sea

as an indicator for long distance transport of fine-grained material. *Baltica*, **16**, 31–36.

de Lugt, I. (2007) Stratigraphical and structural setting of the Palaeogene siliciclastic sediments in the Dutch part of the North Sea Basin. PhD thesis, University of Utrecht, The Netherlands, 112 pp.

Mangerud, J. and Jansen, E. (1996) Late Cenozoic history of the Scandinavian and Barents Sea ice sheets. *Global and Planetary Change*, **12**, 11–26.

Meunier, A. (2007) Soil hydroxy-interlayered minerals: A re-interpretation of their crystallochemical properties. *Clays and Clay Minerals*, **55**, 380–388.

Meunier, A. and Velde, B.D. (2004) *Illite – Origins, Evolution and Metamorphism*. Springer Verlag, Berlin, 288 pp.

Millot, G. (1971) *Geology of Clays. Weathering, Sedimentology, Geochemistry*. Springer-Verlag, Berlin, 429 pp.

Moore, D.M. and Reynolds, J. (1997) *X-Ray Diffraction and the Identification and Analysis of Clay Minerals*. Oxford University Press, New York, 378 pp.

Moreau, J. and Huuse, M. (2014) Infill of tunnel valleys associated with landward-flowing ice sheets: The missing Middle Pleistocene record of the NW European rivers? *Geochemistry, Geophysics, Geosystems*, **15**, 1–9.

Moreau, J., Huuse, M., Janszen, A., van der Vegt, P., Gibbard, P.L., and Moscariello, A. (2012) The glaciogenic unconformity of the southern North Sea. Pp. 99–110 in: *Sediment Provenance Studies in Hydrocarbon Exploration and Production* (R.A. Scott, H.R. Smyth, A.C. Morton and N. Richardson, editors). Special Publications, **368**, Geological Society, London.

Murton, D.K. and Murton, J.B. (2012) Middle and Late Pleistocene glacial lakes of lowland Britain and the southern North Sea Basin. *Quaternary International*, **260**, 115–142. Elsevier Ltd, Amsterdam, and INQUA.

Nielsen, O.L.E.B., Rasmussen, E.S., and Thyberg, B.I. (2015) Distribution of clay minerals in the Northern North Sea Basin during the Paleogene and Neogene: A result of source-area geology and sorting processes. *Journal of Sedimentary Research*, **85**, 562–581.

Norrish, K. and Pickering, J.G. (1983) Clay minerals. Pp. 281–308 in: *Soils, an Australian Viewpoint*. Division of Soils, CSIRO, Academic Press, London.

Novikoff, A., Tsawlassou, U., Gac, J.Y., Bourgeat, F., and Tardy, Y. (1972) Altération des biotites dans les arènes des pays tempérés, tropicaux et équatoriaux. *Sciences Géologiques. Bulletin*, **25**, 287–305.

Petschick, R., Kuhn, G., and Gingele, F. (1996) Clay mineral distribution in surface sediments of the South Atlantic: sources, transport, and relation to oceanography. *International Journal of Marine Geology, Geochemistry and Geophysics*, **130**, 203–229.

Pouchou, J.L. and Pichoir, F. (1984) A new model for quantitative analyses. I. Application to the analysis of homogeneous samples. *La Recherche Aérospatiale*, **3**, 13–38.

Pouchou, J.L. and Pichoir, F. (1985) "PAP" (φ–ρ–) correction procedure for improved quantitative microanalysis. Pp. 104–106 in: *Microbeam Analysis* (J.T. Armstrong, editor). San Francisco Press, San Francisco, California, USA.

Praeg, D. (1996) Morphology, stratigraphy and genesis of buried Mid-Pleistocene tunnel-valleys in the Southern North Sea Basin. PhD thesis, University of Edinburgh, UK, 207 pp.

Ramseyer, K. and Boles, J.R. (1986) Mixed-layer illite/smectite minerals in Tertiary sandstones and shales, San Joaquin Basin, California. *Clays and Clay Minerals*, **34**, 115–124.

Reynolds, R.C. and Hower, J. (1970) The nature of interlayering in mixed-layer illite-montmorillonites. *Clays and Clay Minerals*, **18**, 25–36.

Rieder, M., Cavazzini, G., D'yakonov, Y.S., Frank-Kamenetskii, V.A., Gottardi, G., Guggenheim, S., Koval', P.V., Mueller, G., Neiva, A.M.R., Radoslovich, E.W., Robert, J.-L., Sassi, F.P., Takeda, H., Weiss, Z., and Wones, D.R. (1998) Nomenclature of the micas. *The Canadian Mineralogist*, **36**, 905–912.

Sayles, F.L. (1981) The composition and diagenesis of interstitial solutions – II. Fluxes and diagenesis at the water-sediment interface in the high latitude North and South Atlantic. *Geochimica et Cosmochimica Acta*, **45**, 1061–1086.

Sayles, F.L. and Mangelsdorf Jr., P.C. (1977) The equilibration of clay minerals with sea water: exchange reactions. *Geochimica et Cosmochimica Acta*, **41**, 951–960.

Schaetzl, R. and Thompson, M.L. (2015) *Soils: Genesis and Geomorphology*. 2nd edition. Cambridge University Press, Cambridge, UK, 795 pp.

Schultz, L.G., Shepard, A.O., Blackmon, P.D., and Starkey, H.C. (1971) Mixed–layer kaolinite-montmorillonite from the Yucatan Peninsula, Mexico. *Clays and Clay Minerals*, **19**, 137–150.

Sengupta, P., Saikia, P.C., and Borthakur, P.C. (2008) SEM-EDX characterization of an iron-rich kaolinite clay. *Journal of Scientific and Industrial Research*, **67**, 812–818.

Shell (1993) *K14-12 end of well report: NLOG_GS_PUB_9409_IG8098006_K14-12*. 10 pp.

Smoot, T.W. (1960) *Clay Mineralogy of Pre-Pennsylvanian Sandstones and Shales of the Illinois Basin, Part I. Relation of Permeability to Clay Mineral Suite*. Illinois State Geological Survey, USA, 20 pp.

Środoń, J. (2006) Identification and quantitative analysis of clay minerals. Pp. 767–787 in: *Handbook of Clay Science* (F. Bergaya, B.K.G. Theng, and G. Lagaly, editors). Developments in Clay Science, Elsevier, Amsterdam.

Suquet, H., De la Calle, C., and Pezerat, H. (1975) Swelling and structural organization of saponite. *Clays and Clay Minerals*, **23**, 1–9.

Thorez, J. (1989) Between the crystal and the solutions. A graphical overview of the passage to, from and of the clay minerals in the lithosphere during weathering. Pp. 49–120 in: *Weathering; Its Products and Deposits. Processes* (V.P. Evangelou, G. Faure, J. Goni, P.L.C. Grubb, P.A. Hill, O. Lahondney-Sarc, A.J. Melfi, E. Mendelovici, A.P. Nikitina, W.F. Pickering, and S.S. Augustithis, editors). Theophrastus Publishers S. A., Greece.

Uzarowicz, Ł., Šegvić, B., Michalik, M., and Bylina, P. (2012) The effect of hydrochemical conditions and pH of the environment on phyllosilicate transformations in the weathering zone of pyrite-bearing schists in Wieściszowice (SW Poland). *Clay Minerals*, **47**, 401–417.

van der Vegt, P., Janszen, A., and Moscariello, A. (2012) Tunnel valleys: Current knowledge and future perspectives. Pp. 75–97 in: *Sediment Provenance Studies in Hydrocarbon Exploration and Production* (R.A. Scott, H.R. Smyth, A.C. Morton and N. Richardson, editors). Special Publications, **368**, Geological Society, London.

Warr, L.N. and Rice, A.H.N. (1994) Interlaboratory standardization and calibration of clay mineral crystallinity and crystallite size data. *Journal of Metamorphic Geology*, **12**, 141–152.

Weaver, C.E. and Beck, K.C. (1971) Clay-water diagenesis during burial or how mud becomes gneiss. *Geological Society of America Special Papers*, **134**, 1–78.

Welton, J.E. (1984) *SEM Petrology Atlas*. The American Association of Petroleum Geologists. Methods in Exploration Series, **4**, Tulsa, Oklahoma, USA.

Westerhoff, W. (2009) Stratigraphy and sedimentary evolu-

tion: The lower Rhine-Meuse system during the Late Pliocene and Early Pleistocene (southern North Sea Basin). PhD thesis, University of Amsterdam, The Netherlands.

Whitney, D.L. and Evans, B.W. (2010) Abbreviations for names of rock-forming minerals. *American Mineralogist*, **95**, 185–187.

Whittig, L.D. and Jackson, M.L. (1955) Mineral content and distribution as indexes of weathering in the Omega and Ahmeek soils of Northern Wisconsin. *Clays and Clay Minerals*, **4**, 362–371.

Zagwijn, W.H. (1989) The Netherlands during the Tertiary and the Quaternary: A case history of coastal lowland evolution. *Geologie en Mijnbouw*, **68**, 107–120.

Zuther, M., Brockamp, O., and Clauer, N. (2000) Composition and origin of clay minerals in Holocene sediments from the south-eastern North Sea. *Sedimentology*, **47**, 119–134.

(*Received 4 September 2015; revised 4 April 2016; Ms. 1032; AE: P. Schroeder*)